Supporting Information to

Charge Transfer and Polarisability in Ionic Liquids: A Case Study

Frederik Philippi[a], Kateryna Goloviznina[b], Zheng Gong[b], Sascha Gehrke[c,d], Barbara Kirchner[c], Agílio A. H. Pádua[b], Patricia A. Hunt[a,e]

[a]Department of Chemistry, Molecular Sciences Research Hub, Imperial College London, White City Campus, London W12 0BZ, UK

[b]Laboratoire de Chimie, École Normale Supérieure de Lyon & CNRS, 69364 Lyon, France

[c]Mulliken Center for Theoretical Chemistry, University of Bonn, Beringstr. 4+6, D-53115 Bonn, Germany

[d]Department of Physics and Astronomy, University College London, London, WC1E 6BT United Kingdom

[e]School of Chemical and Physical Sciences, Victoria University of Wellington, Wellington, New Zealand

Contents

1. Abbreviations

We use the nomenclature of the Cl&P force field on which we based our simulations, with a,b,c added to distinguish between sites that are treated together in Cl&P, Figure S1.
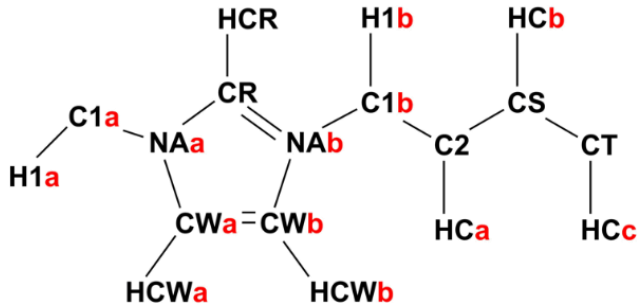
Figure S1: Abbreviations used in this work, following the nomenclature of the CL&P / CL&Pol force fields.

2. Charge Scaling Details

In the atom wise charge scaling formalism used in this work, the charge q_i on an atom i (i.e. an atomic site used in the MD simulation) is obtained using equation (S1).

$$q_i = \Delta q_{total}\left(q_i^{neutral} - q_i^{charged}\right) + q_i^{charged} \tag{S1}$$

Here, Δq_{total} is the total charge transfer on the molecular ion, which is a number between 0 and 1, usually around 0.2. Δq_{total} is related to the more commonly used charge scaling factor as $S = 1 - \Delta q_{total}$, hence $\Delta q_{total} = 0.2$ corresponds to a scaling factor of 0.8. Summing up the atomic charge yields equation (S2) for the charge on a molecular ion consisting of N atoms. Thus, the total charge Q^{scaled} on this molecular ion with charge transfer is given by equation (S3).

$$Q^{scaled} = \sum_i^N q_i \tag{S2}$$

$$
\begin{aligned}
Q^{scaled} = \sum_i^N q_i &= \sum_i^N \left\{ \Delta q \left(q_i^{neutral} - q_i^{charged} \right) + q_i^{charged} \right\} \\
&= \Delta q \sum_i^N \left(q_i^{neutral} - q_i^{charged} \right) + \sum_i^N q_i^{charged} \\
&= \Delta q \left(\sum_i^N q_i^{neutral} - \sum_i^N q_i^{charged} \right) + \sum_i^N q_i^{charged}
\end{aligned}
\tag{S3}
$$

The total charges Q for the two limiting cases are known, i.e. the neutral radical with the total charge 0 and the native molecular ion with a charge of ±1, equation (S4) and (S5).

$$\sum_i^N q_i^{neutral} = Q^{neutral} = 0 \tag{S4}$$

$$\sum_i^N q_i^{charged} = Q^{charged} = \pm 1 \tag{S5}$$

Thus, inserting (S4) and (S5) into (S3), it is clear that the total charge Q^{scaled} on the molecular ion obtained from the sum of the atom wise scaled charges analytically fulfils the requirements $Q^{scaled} = 1 - \Delta q$ (for the cation) and $Q^{scaled} = -1 + \Delta q$ (for the anion), see equation (S6).

$$Q^{scaled} = \sum_{i}^{N} q_i = Q^{charged} - \Delta q Q^{charged} \tag{S6}$$

3. Simulation Densities

Averaged box sizes for the different simulation setups are given in Table S1. The uncertainty in the density is calculated by gaussian error propagation from the standard deviation in the box size, which in turn is accessible from the > 10 repeats of the averaging procedure described in the main manuscript.

Table S1: Cell sizes for the different simulation types and resulting density. The last column gives the deviation from the experimental value of 1.403 g/mL.[1]

	Box size / Å		Density / g mL^{-1}		Deviation
	Mean	Standard Deviation	value	uncertainty	
CL&P	63.23	0.02	1.411	0.002	0.5%
Cl&P scaled	63.59	0.02	1.387	0.001	-1.2%
CL&P-MSK	63.26	0.02	1.408	0.001	0.4%
CL&P-MSK scaled	63.59	0.02	1.387	0.001	-1.1%
CL&P-CHELPG	63.26	0.03	1.408	0.002	0.4%
CL&P-CHELPG scaled	63.61	0.02	1.385	0.002	-1.3%
Cl&P-ADCH	63.31	0.02	1.405	0.001	0.1%
Cl&P-ADCH scaled	63.66	0.02	1.382	0.001	-1.5%
CL&P+Drude/NH (C-H not fix)	64.05	0.01	1.357	0.001	-3.3%
CL&P+Drude/NH	63.48	0.02	1.394	0.001	-0.7%
CL&P+Drude/TG-NH	63.18	0.04	1.414	0.003	0.8%
CLPOL/TG-NH	63.76	0.02	1.376	0.001	-1.9%

4. CL&P force field thermostat considerations

Drude induced dipoles allow the introduction of polarizability into classical MD simulations. However, there are specific difficulties related to the use of thermostats and the impact of constraining the C-H dynamics that need to be explored.

The extended Lagrangian approach used in this work requires thermostatting to control the temperature (NVT ensemble). However, the use of a temperature control algorithm can affect the dynamics of a system.[2,3] **Table S2** collects information from a series of simulations (employing the non-polarized CL&P potential). The effect on dynamics can be quantified by comparing the diffusion coefficients (D_{self}). The global Nosé-Hoover thermostat in this work has been shown to reproduce the dynamics of an NVE ensemble.[3] This result is confirmed by comparison of simulations A and B/C in **Table S2**. Diffusion of the ions within the NVE ensemble (simulation A), does not differ significantly from the diffusion in the two NVT ensembles with τ = 100 fs, simulation B), and τ = 25 fs, (simulation C). While these results are obtained from the nonpolarizable force field, they clearly show that the type of thermostat and the chosen damping timescale are not disturbing the dynamics.

Table S2: Self-diffusion coefficients (D) for the cations (C), anions (A), and their ratio DC/DA from MD simulations. Each value is an average of 10 separate runs with of 10 ns each, fitted from 3-7 ns. Errors at the 95% confidence level given in brackets were obtained from the standard deviation over the 10 averages.

Simulation	A	B	C	D
Fixed C-H bonds	Yes	Yes	Yes	No
Ensemble	NVE	NVT (τ=100 fs)	NVT (τ=25 fs)	NVE
D_{self}^{cation} / 10^{-8} cm²/s	9.4(6)	9.8(5)	9.8(5)	10.1(4)
D_{self}^{anion} / 10^{-8} cm²/s	6.6(6)	7.1(4)	6.9(3)	7.4(5)
D_{self}^{cation} / D_{self}^{anion}	1.4(2)	1.4(2)	1.4(1)	1.4(1)

C-H bond vibrations are generally the fastest modes in a simulation. The timescale of this motion can be estimated using the Einstein period, **Eqn (S7)**[4] with the mass m of a hydrogen atom and the force constant k of the harmonic potential $E = kx^2$. in this work, the Einstein period is 0.6 fs. In contrast, the Einstein period of a C-C vibration is approximately 2-3 fs. Thus, a timestep of 1 fs is too long to describe the C-H vibrations accurately (**Table S2**, simulation D) and the C-H bonds are typically constrained using the SHAKE algorithm (**Table S2**, simulation A). These approximations lead to a small drift in the total energy (which should be constant) of less than 0.1% over 10 ns for both simulations, **ESI Section 5**. The bias introduced is comparable to the error in the diffusion coefficients and no difference in the relative quantity D_{self}^{cation} / D_{self}^{anion} is found.

$$t_E = \pi \sqrt{\frac{6m}{k}} \qquad \text{(S7)}$$

5. Energy drift

The energy drift was negligible in all test simulations using the unscaled CL&P force field, see Table S3 to Table S7 below for the fit parameters of a linear fit of the total energy. The total energy values used in the fit were written every 1 ps over the course of the 10 ns simulation. Several repeats were performed.

Table S3: Microcanonical ensemble NVE, no fixed bonds.

Intercept / kcal mol⁻¹		Slope / kcal mol⁻¹ fs⁻¹		
Value	Error	Value	Error	Drift over 10 ns
21522.18	0.06	1.68E-06	9.64E-09	0.08%
21646.52	0.06	1.14E-06	9.57E-09	0.05%
21714.17	0.05	1.61E-06	9.44E-09	0.07%
21656.05	0.06	1.04E-06	1.10E-08	0.05%
21807.34	0.05	1.48E-06	9.35E-09	0.07%
21667.25	0.06	1.53E-06	9.53E-09	0.07%
21396.12	0.05	7.20E-07	9.19E-09	0.03%
21570.87	0.05	8.68E-07	9.21E-09	0.04%
21686.15	0.05	1.47E-06	9.31E-09	0.07%
21606.69	0.06	2.10E-06	9.59E-09	0.10%

Table S4: Microcanonical ensemble NVE, C-H bonds were constrained using the SHAKE algorithm with 20 iterations.

Intercept / kcal mol⁻¹		Slope / kcal mol⁻¹ fs⁻¹		
Value	Error	Value	Error	Drift over 10 ns
16431.58	0.02	-1.04E-06	3.83E-09	-0.06%
16394.77	0.03	-1.47E-06	5.26E-09	-0.09%
16531.32	0.02	-6.59E-07	3.98E-09	-0.04%

16671.79	0.03	-1.17E-06	4.44E-09	-0.07%
16536.93	0.03	-1.55E-06	4.67E-09	-0.09%
16019.47	0.03	-2.19E-06	4.81E-09	-0.14%
16372.23	0.02	-8.05E-07	3.79E-09	-0.05%
16224.36	0.03	-1.13E-06	5.97E-09	-0.07%
15975.44	0.02	-5.06E-07	3.99E-09	-0.03%
16166.76	0.02	-4.97E-07	4.27E-09	-0.03%

Table S5: Microcanonical ensemble, C-H bonds were constrained using the SHAKE algorithm with 100 iterations.

Intercept / kcal mol^{-1}		Slope / kcal mol^{-1} fs^{-1}		
Value	Error	Value	Error	Drift over 10 ns
16491.18	0.02	-1.02E-06	3.80E-09	-0.06%
16394.77	0.03	-1.47E-06	5.26E-09	-0.09%
16531.32	0.02	-6.59E-07	3.98E-09	-0.04%
16671.79	0.03	-1.17E-06	4.44E-09	-0.07%
16536.93	0.03	-1.55E-06	4.67E-09	-0.09%
16019.47	0.03	-2.19E-06	4.81E-09	-0.14%
16209.18	0.03	-2.10E-07	4.84E-09	-0.01%
16166.76	0.02	-4.97E-07	4.27E-09	-0.03%
15975.44	0.02	-5.06E-07	3.99E-09	-0.03%

Table S6: Canonical ensemble, C-H bonds were constrained using the SHAKE algorithm with a maximum of 20 iterations. NVT damping parameter was 100 fs.

Intercept / kcal mol^{-1}		Slope / kcal mol^{-1} fs^{-1}		
Value	Error	Value	Error	Drift over 10 ns
16345.70	3.16	-2.41E-06	5.48E-07	-0.15%
16325.47	3.18	4.54E-07	5.50E-07	0.03%
16349.56	3.17	-1.81E-06	5.49E-07	-0.11%
16341.28	3.14	-2.79E-06	5.44E-07	-0.17%
16349.33	3.16	-1.18E-06	5.47E-07	-0.07%
16333.22	3.15	8.22E-07	5.46E-07	0.05%
16341.34	3.17	-4.64E-07	5.49E-07	-0.03%

Table S7: Canonical ensemble, C-H bonds were constrained using the SHAKE algorithm with 20 iterations. NVT damping parameter was 25 fs.

Intercept / kcal mol^{-1}		Slope / kcal mol^{-1} fs^{-1}		
Value	Error	Value	Error	Drift over 10 ns
16350.15	3.14	-2.62E-06	5.43E-07	-0.16%
16339.07	3.17	-2.42E-06	5.49E-07	-0.15%
16331.01	3.15	6.17E-07	5.45E-07	0.04%
16322.18	3.18	4.70E-06	5.51E-07	0.29%
16345.38	3.15	-2.86E-06	5.46E-07	-0.17%
16309.61	3.15	3.12E-06	5.46E-07	0.19%
16314.32	3.15	1.10E-06	5.46E-07	0.07%
16313.37	3.18	2.53E-06	5.50E-07	0.16%
16320.99	3.17	1.68E-06	5.50E-07	0.10%
16313.10	3.16	3.41E-06	5.48E-07	0.21%

6. CL&Pol implementation

In CL&Pol the LJ potential is modified to avoid double counting of Drude-particle recovered polarisation effects (https://github.com/paduagroup/clandpol). The LJ potential models Pauli repulsion and long-range attractive interactions (Van der Waals) via empirical fitting. The components of the Van der Waals interaction include Keesom (permanent charge and permanent multipole-multipole) Debye (dipole-induced dipole (multipole), induction) and London (induced dipole-induced dipole (multipole), dispersion) forces. The Drude particle formalism recovers a portion of these interactions which therefore must be removed from the LJ-parameters.

LJ parameter well depths inherited from the CL&P database were scaled down as defined in **Eqn** (S8). The k_{ij} scaling factors are evaluated from symmetry-adapted perturbation theory (SAPT),[5,6] or from a predictive scheme outlined in ref. [7]. In order to achieve transferability of the force field, the scaling factors k_{ij} are evaluated for interactions between ion-fragments (for example, short neutral alkyl chain, ionic head group) and not entire ions. The fragments employed were 1-ethyl-3-methylimidazolium ($C_2C_1im^+$), butane (C_4H_{10}) and bis(trifluoromethanesulfonyl)amide ([NTf_2]$^-$), scaling factors are given in Table S8.[7]

$$k_{ij} = \frac{E_{disp}}{E_{disp} + E_{ind}} \qquad (S8)$$

Table S8: Scaling coefficients for modification of non-bonded attractive energies.

Dimer	k_{ij}
[C_2C_1im]$^+$···[NTf_2]$^-$	0.65
[C_2C_1im]$^+$···C_4H_{10}	0.76
[NTf_2]$^-$···C_4H_{10}	0.77
C_4H_{10}···C_4H_{10}	0.94

7. Temperature grouped thermostat TG-NH

The Drude polarizable simulations use an extended Lagrangian approach, where the motion of the "atoms" (A) which are the centre of mass (CoM) of the Drude core-particle pairs, is thermostatted at T_A=333 K, while the relative motion between the Drude core-particle pairs is thermostatted at T_D=1 K.[8] A Nose-Hoover (NH) thermostat is employed.

There is heat flow from the high frequency atom motions (such as C-H vibrations) into the high frequency Drude core-particle pair motion. Loss of kinetic energy from high frequency modes leads to an uneven distribution of kinetic energy in the system, violating the equipartition theorem (requiring equal distribution of kinetic energy in all unconstrained motions).[9] The kinetic energy distribution is now weighted towards the low-frequency motions of the "atoms", leading to a too high molecular CoM translational motion and an underestimation of the density which combine to result in an overestimation of diffusion. The high molecular CoM motion leads to a too high effective translational temperature relative to the set thermostat.

The newly implemented temperature-grouped Nose-Hoover thermostat (TG-NH) solves this problem by thermostatting the molecular centre of mass motions seperately.[9] Thus, the TG-NH thermostat is made of three independent thermostats applied to (a) molecular (M) centre of mass (CoM) motions, (b) the motion of the centre of mass of the core-Drude particle pairs (atoms A) relative to the MCoM and (c) motions of Drude-particle relative to the Drude-core for each pair (D). The MCoM and ACoM are thermalised at 333K while the Drude core-particle pairs are thermalised at 1K. In the TG-NH scheme simulations carried out for this work the temperature damping parameter τ was set to 100 fs for the real degrees of freedom and 25 fs for the Drude core - Drude particle pairs.[10] See also Section 4 for a comparison of damping parameters for the non-polarisable force fields. This method is denoted as the temperature grouped NH scheme (TG-NH).

8. Conformational space covered by sampled structures

The 512 structures dumped from an equilibrated MD simulation reasonably cover the conformational space for both cation and anion. The anion conformers are characterised by their two backbone C-S-N-S dihedral angles, see Figure S2 plotted with the *ab-initio* potential energy surface, and Figure S3 as overlay of all structures. The overlay of all structures / conformers of the cation are shown in Figure S4. The conformational space covered by the side chain is characterised by the three dihedrals that determine the conformation of the side chain, see the histograms in Figure S5, Figure S6, Figure S7. The converged histograms for the full production run trajectories for the different force fields are shown for comparison.
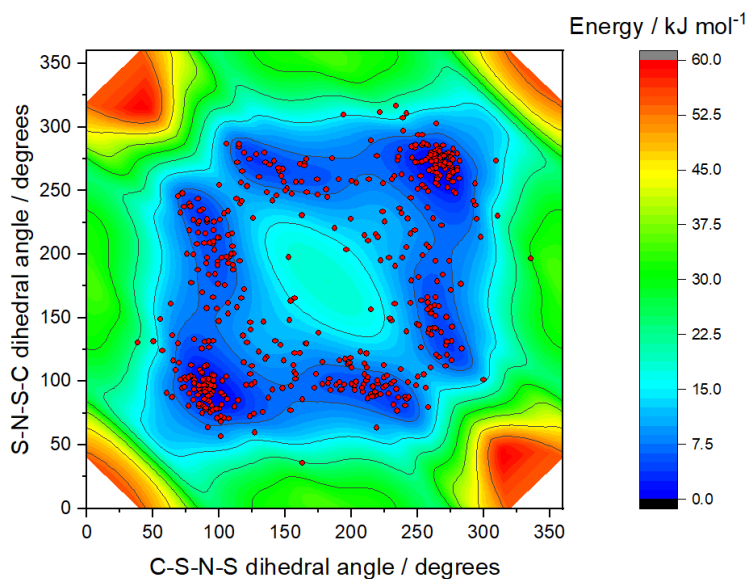
Figure S2: The 512 anion structures extracted from the MD simulation reasonably cover the available conformational space. For comparison, the *ab-initio* potential energy surface is also shown.
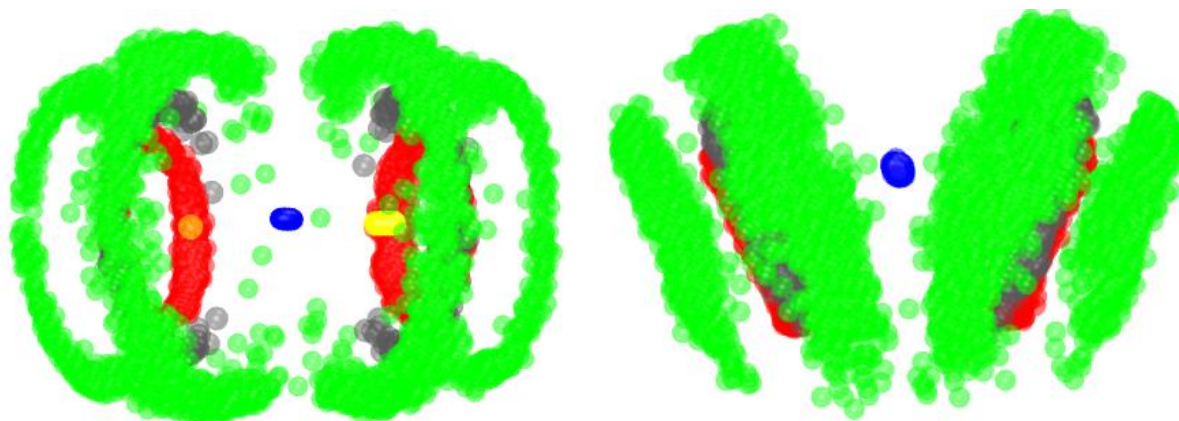
View along the nitrogen atom and the middle of the sulphur atoms.

View normal to the plane spanned by N,S,S

Figure S3: Overlay of the different conformers of [NTf₂]⁻ in the 512 sampled structures.
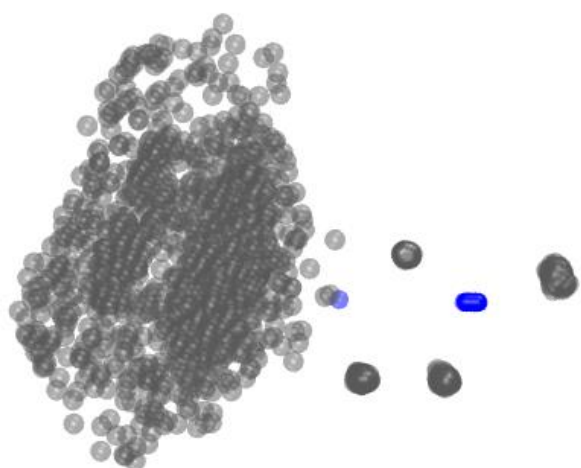
View normal to the ring plane
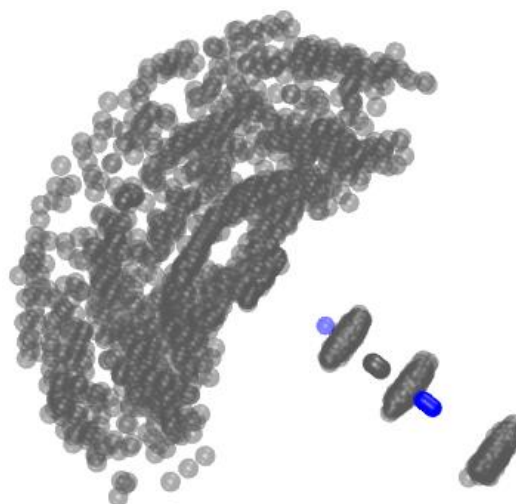
View along the CR atom and the middle of the CWa/CWb atoms.

Figure S4: Overlay of the different conformations of [C$_4$C$_1$im]$^+$ in the 512 sampled structures. Hydrogen atoms omitted for clarity.
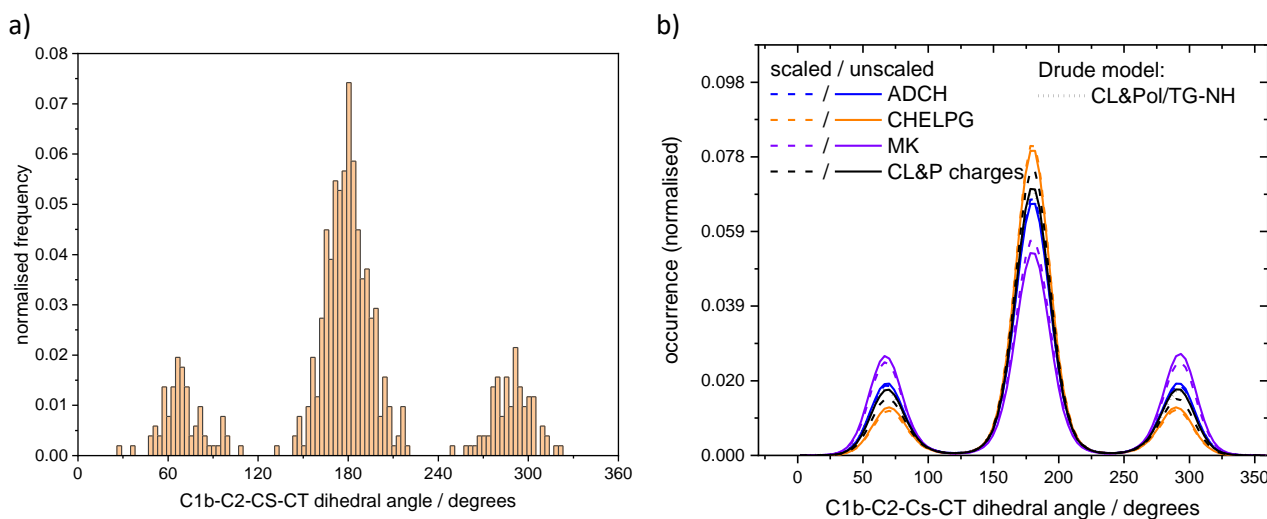
Figure S5: a) Histogram of the dihedral angle corresponding to rotation around the C2-CS bond in the BMIM cation for the 512 cation structures extracted from the MD simulation. For comparison, b) the corresponding histograms over all 5120000 structures in the trajectories.
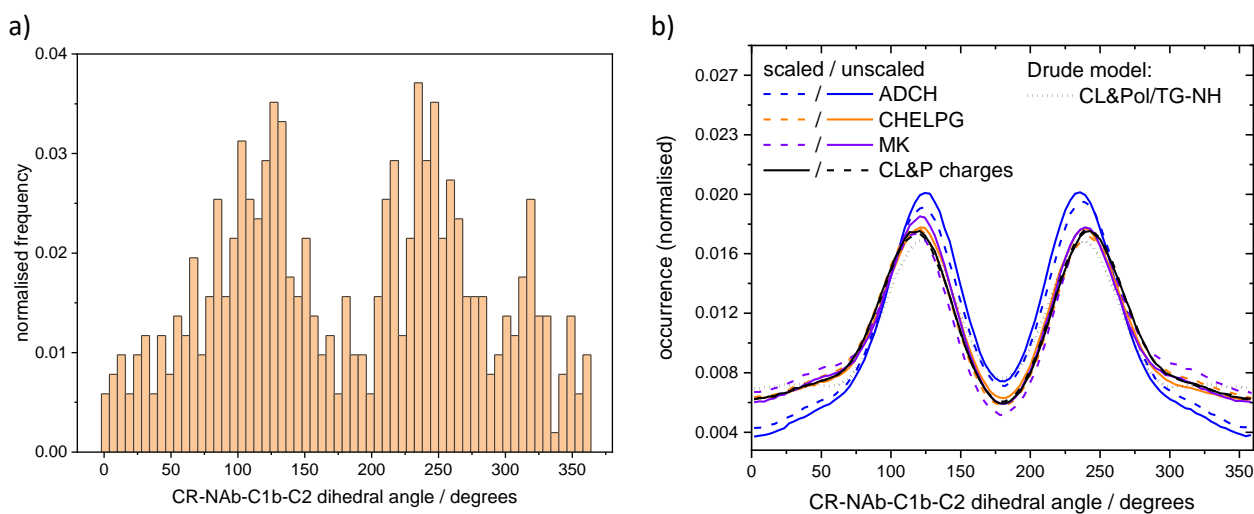
Figure S6: a) Histogram of the dihedral angle corresponding to rotation around the NAb-C1b bond in the BMIM cation for the 512 cation structures extracted from the MD simulation. b) the corresponding histograms over all 5120000 structures in the trajectories.
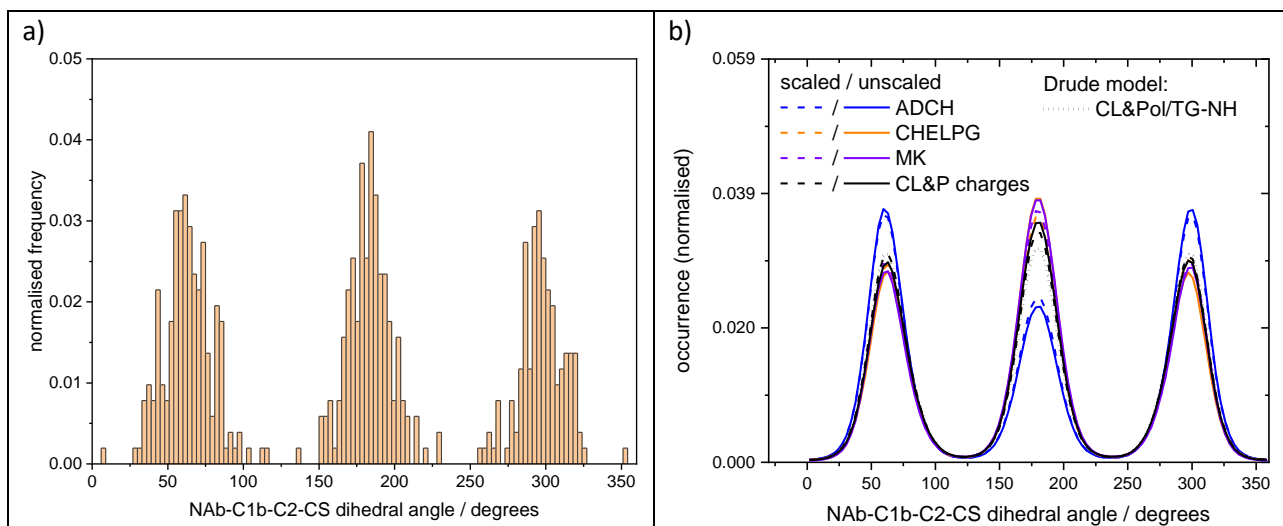
Figure S7: a) Histogram of the dihedral angle corresponding to rotation around the C1b-C2 bond in the BMIM cation for the 512 cation structures extracted from the MD simulation. b) the corresponding histograms over all 5120000 structures in the trajectories.

9. Influence of a solvation model on atomic charges

To investigate the influence of charge redistribution in the presence of a polarisable continuum, we calculated the CHELPG charges for the 512 $[NTf_2]^-$ structures using the SMD parameters for $[C_4C_1im][NTf_2]$.[11] The difference was negligible, Figure S8.
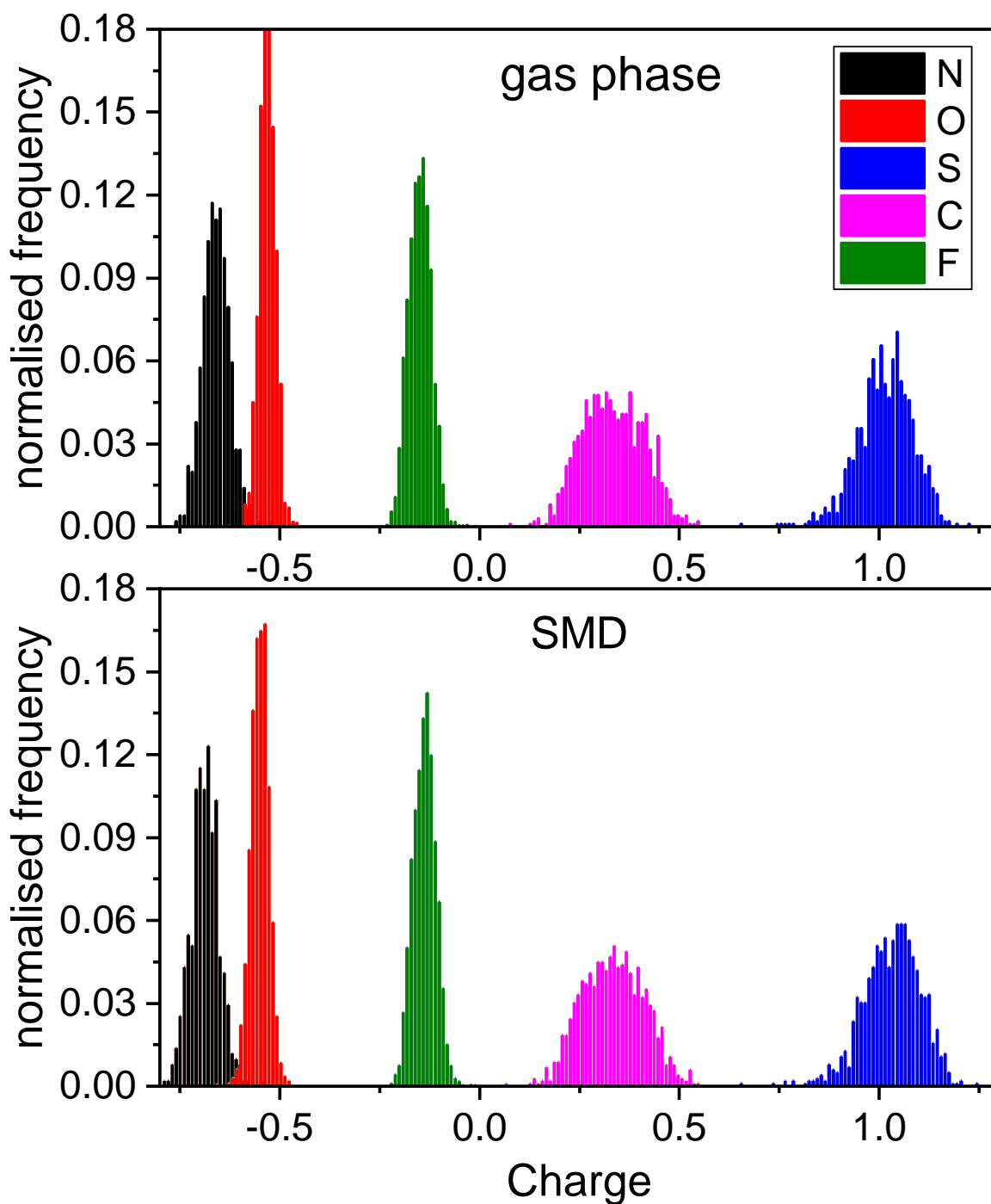
Figure S8: Comparison of charge distribution histograms for the gas phase and SMD models.

10.   Derivation of the theoretical charge transfer

The ease of which charge is transferred between chemical systems can be quantitatively described using the derivatives of the energy E with respect to the number of electrons N in the form of a Taylor expansion, **Eqn (S9)**. The first two derivatives are the chemical potential of the electrons μ and the hardness η, **Eqn (S10) and Eqn (S11)**.[12]

$$E(N) \approx E_{N_0} - \mu(N - N_0) + \eta(N - N_0)^2 \tag{S9}$$

$$\mu = -\left(\frac{\partial E}{\partial N}\right)_v \tag{S10}$$

$$\eta = \frac{1}{2}\left(\frac{\partial^2 E}{\partial N^2}\right)_v \tag{S11}$$

The chemical potential of the electrons and the hardness are obtained in the finite difference approximation from the energies E of the vertical ionisation processes as shown in (S12) and (S13).[12] Calculations with convergence failures were excluded, in any case at least 487 out 512 structures converged without issues. The subscripts correspond to the native, singly charged cations and anions (E_{N_0}), the radicals with one electron removed (E_{N_0-1}), and the radicals with one electron added (E_{N_0+1}).

$$\mu = \frac{E_{N_0-1} - E_{N_0+1}}{2} \tag{S12}$$

$$\eta = \frac{E_{N_0-1} + E_{N_0+1} - 2E_{N_0}}{2} \tag{S13}$$

For cations C and anions A, this leads to Eqn (S14) and (S15) for their change in energy as a function of the charge transfer Δq.

$$dE^C(N) = -\mu^C(dN) + \eta^C(dN)^2 = -\mu^C(\Delta q) + \eta^C(\Delta q)^2 \tag{S14}$$

$$dE^A(N) = -\mu^A(dN) + \eta^A(dN)^2 = +\mu^A(\Delta q) + \eta^A(\Delta q)^2 \tag{S15}$$

We will consider vertical ionisation processes, i.e. the external potential v provided by the nuclei is kept constant. For ILs, electrostatic forces dominate the interaction energy in the bulk and part of this interaction energy is lost if charge transfer occurs. Thus, it is necessary to introduce a correction $\Delta E_{Coulomb}$ for this loss in Coulomb attraction, which leads to Eqn (S16) for the total energy:

$$E(N) = -\mu^C\Delta q + \eta^C\Delta q^2 + \mu^A\Delta q + \eta^A\Delta q^2 + \Delta E_{Coulomb} \tag{S16}$$

The electrostatic interaction energy $\Delta E_{Coulomb}$ between the ions is estimated considering the ions as point charges, Eqn (S17).

$$\Delta E_{Coulomb} = \frac{-\alpha e^2(1 - \Delta q)^2}{4\pi\varepsilon_0 d} \tag{S17}$$

Where e is the elementary charge, d the distance between ions and ε_0 the vacuum permittivity. The Madelung constant α is used to include the effects of bulk structure. The interaction energy $\Delta E_{Coulomb}$ of an ion pair in this simple picture is recovered for $\alpha = 1$. To find the charge transfer for which the total energy is minimised, the first derivative is set to zero, Eqn (S18).

$$\frac{dE(N)}{d(\Delta q)} = -\mu^C + 2\eta^C\Delta q + \mu^A + 2\eta^A\Delta q + \frac{2\alpha e^2(1 - \Delta q)}{4\pi\varepsilon_0 d} = 0 \tag{S18}$$

Which leads to the final form of the charge transfer equation, Eq (S19).

$$\Delta q = \frac{\mu^C - \mu^A - \frac{\alpha e^2}{2\pi\varepsilon_0 d}}{2\eta^C + 2\eta^A - \frac{\alpha e^2}{2\pi\varepsilon_0 d}} \qquad (S19)$$

The average values for μ and η are given in **Table S9**. The values for $U^C + U^A = \frac{-\alpha e^2}{4\pi\varepsilon_0 d}$ are given in **Section 18** together with the Coulomb interaction fit parameters. We used a distance d=5.5 Å to obtain Δq_{total}=0.36±0.01e (α=0) and Δq_{total}=0.14±0.02e (α=1). The uncertainty in Δq_{total} was estimated using the standard deviations given in **Table S9** and Gaussian standard error propagation methods.

Table S9: μ and η, averaged over the 512 single point calculations for each cation and anion.

	Mean		Standard Deviation	
	kJ/mol	eV	kJ/mol	eV
η^A	495.0	5.13	12.3	0.13
η^C	503.4	5.22	10.5	0.11
μ^A	109.6	1.14	10.2	0.11
μ^C	819.0	8.49	8.6	0.09

11. Atomic charges

The atomic charges evaluated at the UMP2/cc-pVTZ level averaged over symmetrically equivalent atoms are given in Table S10 to Table S14, a summary is given in Figure S9. The atom-wise scaled charges used for the simulations in this work are given in Table S16 and Table S17 for anion and cation, respectively.

Table S10: Average charges and standard deviation for the charged anion [NTf$_2$]$^-$.

	ADCH		CHELPG		NBO		MSK	
Atom_type	average	stddev	average	stddev	average	stddev	average	stddev
N	-0.424	0.025	-0.655	0.034	-1.254	0.016	-0.604	0.038
O	-0.442	0.019	-0.529	0.020	-0.919	0.012	-0.495	0.022
S	0.671	0.011	1.015	0.069	2.203	0.022	0.916	0.075
C	0.414	0.010	0.331	0.077	0.759	0.014	0.284	0.081
F	-0.163	0.018	-0.154	0.028	-0.332	0.011	-0.136	0.029

Table S11: Average charges, standard deviation for the neutral radical [NTf$_2$]$^{\cdot}$.

	ADCH		CHELPG		NBO		MSK	
Atom_type	average	stddev	average	stddev	average	stddev	average	stddev
N	-0.012	0.048	-0.226	0.175	-0.811	0.134	-0.196	0.166
O	-0.328	0.025	-0.354	0.074	-0.789	0.058	-0.325	0.068
S	0.633	0.026	0.837	0.208	2.112	0.029	0.758	0.185
C	0.368	0.017	0.281	0.172	0.787	0.024	0.242	0.161
F	-0.113	0.024	-0.099	0.051	-0.306	0.014	-0.084	0.049

Table S12: Condensed Fukui function f_i^- for the [NTf$_2$]$^-$ Anion.

Atom_type	ADCH	CHELPG	NBO	MSK
N	-0.412	-0.429	-0.443	-0.408
O	-0.114	-0.175	-0.130	-0.170
S	0.038	0.178	0.091	0.158
C	0.046	0.050	-0.028	0.042
F	-0.050	-0.055	-0.026	-0.052

Table S13: Average charges and standard deviation for the charged cation $[C_4C_1im]^+$.

	ADCH		CHELPG		NBO		MSK	
Atom_type	average	stddev	average	stddev	average	stddev	average	stddev
H1a	0.152	0.013	0.146	0.015	0.225	0.009	0.190	0.017
C1a	-0.214	0.022	-0.238	0.045	-0.370	0.015	-0.420	0.054
HCWa	0.199	0.031	0.192	0.012	0.249	0.009	0.228	0.016
NAa	-0.018	0.055	0.151	0.050	-0.259	0.008	0.259	0.070
CWa	-0.085	0.082	-0.117	0.038	-0.034	0.008	-0.184	0.062
CR	0.105	0.117	-0.052	0.052	0.220	0.010	-0.133	0.078
HCR	0.196	0.046	0.184	0.019	0.237	0.009	0.210	0.024
CWb	-0.075	0.081	-0.112	0.047	-0.035	0.009	-0.179	0.071
NAb	-0.012	0.055	0.113	0.075	-0.257	0.008	0.203	0.102
HCWb	0.194	0.031	0.194	0.017	0.250	0.008	0.234	0.022
C1b	-0.103	0.015	-0.097	0.108	-0.181	0.014	-0.248	0.151
H1b	0.127	0.013	0.097	0.028	0.215	0.009	0.143	0.035
C2	-0.167	0.012	0.004	0.115	-0.381	0.013	-0.040	0.147
HCa	0.103	0.023	0.031	0.036	0.204	0.015	0.058	0.043
CS	-0.157	0.016	0.129	0.102	-0.365	0.012	0.117	0.122
HCb	0.087	0.022	-0.010	0.033	0.189	0.013	0.012	0.033
CT	-0.256	0.014	-0.245	0.086	-0.565	0.011	-0.350	0.110
HCc	0.101	0.019	0.073	0.028	0.200	0.013	0.102	0.032

Table S14: Average charges and standard deviation for the neutral radical $[C_4C_1im]^{\bullet}$

	ADCH		CHELPG		NBO		MSK	
Atom_type	average	stddev	average	stddev	average	stddev	average	stddev
H1a	0.098	0.016	0.054	0.032	0.185	0.012	0.105	0.035
C1a	-0.184	0.024	-0.097	0.090	-0.345	0.009	-0.310	0.099
HCWa	0.152	0.036	0.168	0.028	0.214	0.010	0.219	0.035
NAa	-0.022	0.105	0.289	0.120	-0.344	0.018	0.489	0.143
CWa	-0.178	0.106	-0.266	0.142	-0.095	0.087	-0.376	0.175
CR	-0.255	0.219	-0.685	0.181	-0.151	0.073	-0.916	0.225
HCR	0.120	0.089	0.185	0.031	0.199	0.008	0.254	0.042
CWb	-0.157	0.105	-0.266	0.138	-0.107	0.085	-0.353	0.169
NAb	-0.015	0.109	0.264	0.134	-0.350	0.022	0.414	0.166
HCWb	0.147	0.044	0.168	0.032	0.215	0.009	0.219	0.038
C1b	-0.075	0.020	0.006	0.137	-0.158	0.010	-0.141	0.184
H1b	0.082	0.016	0.017	0.047	0.179	0.012	0.064	0.051
C2	-0.154	0.010	0.042	0.157	-0.377	0.010	-0.022	0.179
HCa	0.080	0.012	-0.010	0.043	0.188	0.008	0.021	0.044
CS	-0.143	0.010	0.191	0.133	-0.363	0.010	0.187	0.148
HCb	0.076	0.012	-0.044	0.036	0.185	0.008	-0.021	0.037
CT	-0.257	0.013	-0.234	0.101	-0.565	0.009	-0.349	0.122
HCc	0.084	0.012	0.049	0.027	0.190	0.006	0.081	0.031

Table S15: Condensed Fukui function f_i^+ for the $[C_4C_1Im]^+$ cation

Atom_type	ADCH	CHELPG	NBO	MSK
H1a	-0.054	-0.092	-0.040	-0.085
C1a	0.030	0.141	0.025	0.110
HCWa	-0.047	-0.024	-0.035	-0.009
NAa	-0.004	0.138	-0.085	0.230
CWa	-0.093	-0.149	-0.061	-0.192
CR	-0.360	-0.633	-0.371	-0.783
HCR	-0.076	0.001	-0.038	0.044
CWb	-0.082	-0.154	-0.072	-0.174
NAb	-0.003	0.151	-0.093	0.211
HCWb	-0.047	-0.026	-0.035	-0.015
C1b	0.028	0.103	0.023	0.107
H1b	-0.045	-0.080	-0.036	-0.079
C2	0.013	0.038	0.004	0.018
HCa	-0.023	-0.041	-0.016	-0.037
CS	0.014	0.062	0.002	0.070
HCb	-0.011	-0.034	-0.004	-0.033
CT	-0.001	0.011	0.000	0.001
HCc	-0.017	-0.024	-0.010	-0.021

Table S16: Atom-wise scaled charges for the $[NTf_2]^-$ anion.

	ADCH		CHELPG		NBO		MSK	
Atom_type	average	stddev	average	stddev	average	stddev	average	stddev
N	-0.368	0.028	-0.596	0.043	-1.193	0.026	-0.548	0.045
O	-0.427	0.019	-0.505	0.023	-0.901	0.015	-0.472	0.024
S	0.666	0.012	0.991	0.075	2.190	0.023	0.894	0.080
C	0.408	0.010	0.325	0.081	0.763	0.015	0.278	0.085
F	-0.156	0.018	-0.146	0.029	-0.329	0.012	-0.128	0.030

Table S17: Atom-wise scaled charges for the $[C_4C_1im]^+$ cation.

Atom_type	ADCH		CHELPG		NBO		MSK	
	average	stddev	average	stddev	average	stddev	average	stddev
H1a	0.144	0.014	0.133	0.016	0.220	0.009	0.179	0.018
C1a	-0.210	0.022	-0.219	0.047	-0.366	0.016	-0.405	0.056
HCWa	0.193	0.032	0.189	0.013	0.244	0.010	0.227	0.017
NAa	-0.019	0.057	0.170	0.053	-0.271	0.009	0.291	0.073
CWa	-0.098	0.083	-0.138	0.043	-0.043	0.015	-0.211	0.066
CR	0.055	0.121	-0.139	0.059	0.169	0.017	-0.241	0.085
HCR	0.186	0.048	0.184	0.020	0.232	0.009	0.216	0.025
CWb	-0.086	0.082	-0.134	0.051	-0.045	0.015	-0.203	0.075
NAb	-0.012	0.057	0.134	0.077	-0.270	0.010	0.232	0.105
HCWb	0.188	0.031	0.191	0.018	0.245	0.009	0.232	0.023
C1b	-0.099	0.015	-0.083	0.110	-0.178	0.014	-0.233	0.153
H1b	0.121	0.014	0.086	0.029	0.210	0.009	0.132	0.036
C2	-0.166	0.012	0.009	0.117	-0.380	0.014	-0.038	0.149
HCa	0.100	0.023	0.025	0.037	0.202	0.015	0.052	0.043
CS	-0.155	0.016	0.138	0.104	-0.365	0.012	0.126	0.123
HCb	0.085	0.022	-0.014	0.034	0.189	0.014	0.008	0.034
CT	-0.257	0.015	-0.243	0.087	-0.565	0.012	-0.350	0.112
HCc	0.099	0.020	0.070	0.028	0.199	0.013	0.099	0.033
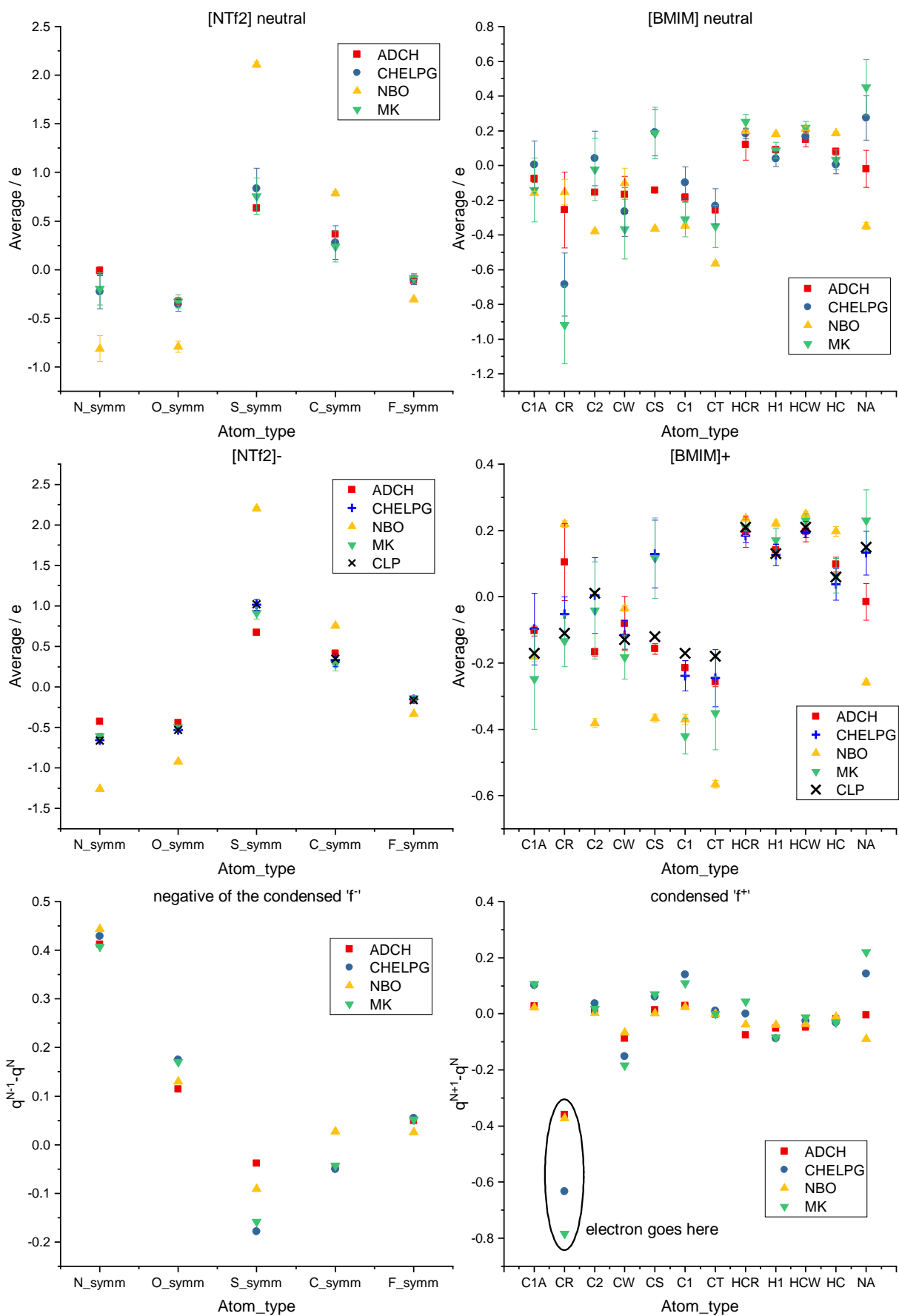
Figure S9: Graphical summary of atomic partial charges.

12. Atomic partial charge histograms

Raw histograms for all atomic partial charge schemes in this work are shown in Figure S10 for the $[NTf_2]^-$ anion and in Figure S11 for the corresponding neutral radical. Figure S12 shows the ADCH, CHELPG, and NBO charge distributions for selected atoms of the $[C_4C_1Im]^+$ cation.
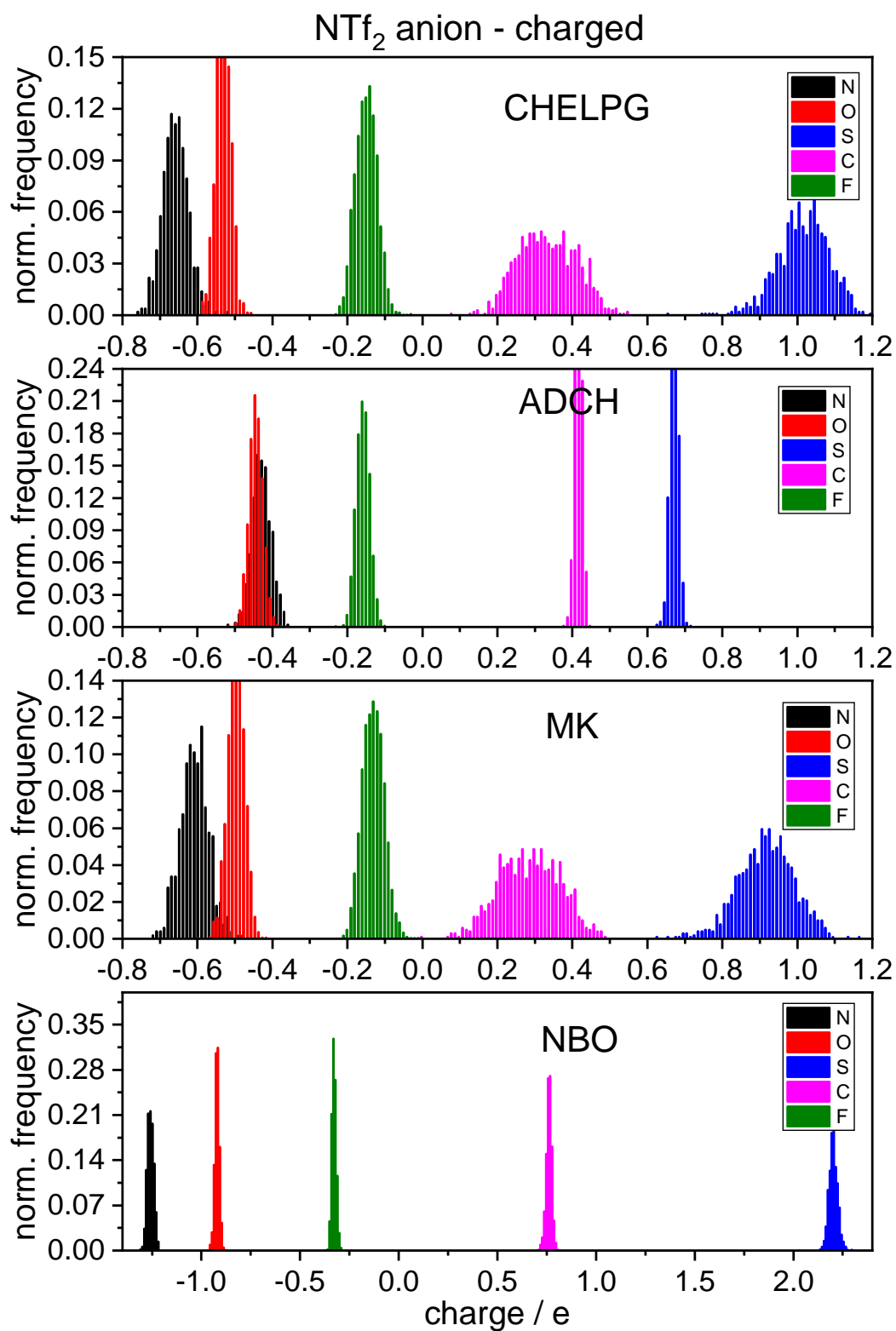
Figure S10: Histogram of atomic charges obtained for the $[NTf_2]^-$ anion using different atomic charge partition schemes for the 512 structures sampled from the MD simulation.
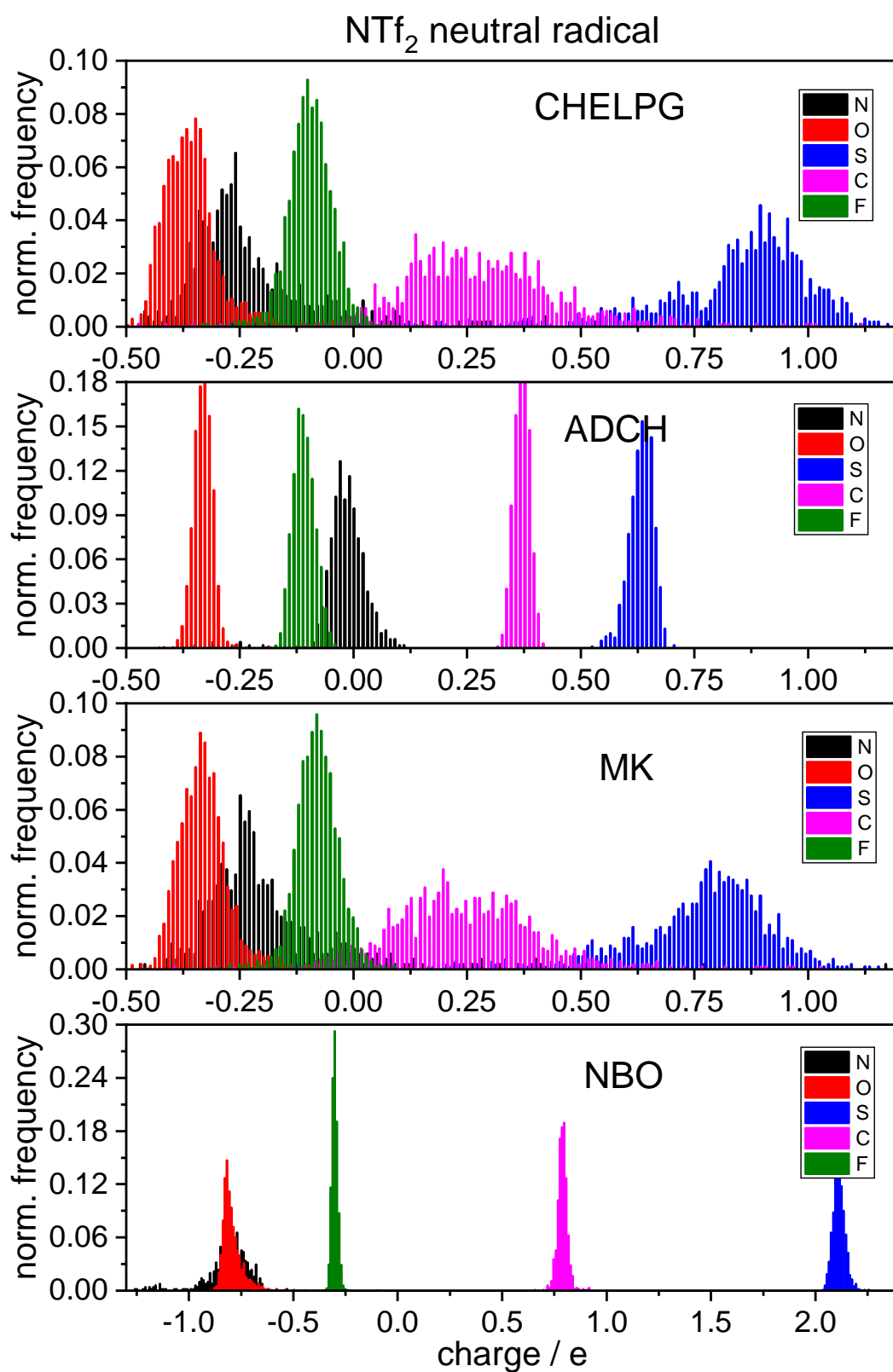
Figure S11: Histogram of atomic charges obtained for the [NTf$_2$]$^{\bullet}$ neutral radical using different atomic charge partition schemes for th 512 structures sampled from the MD simulation.
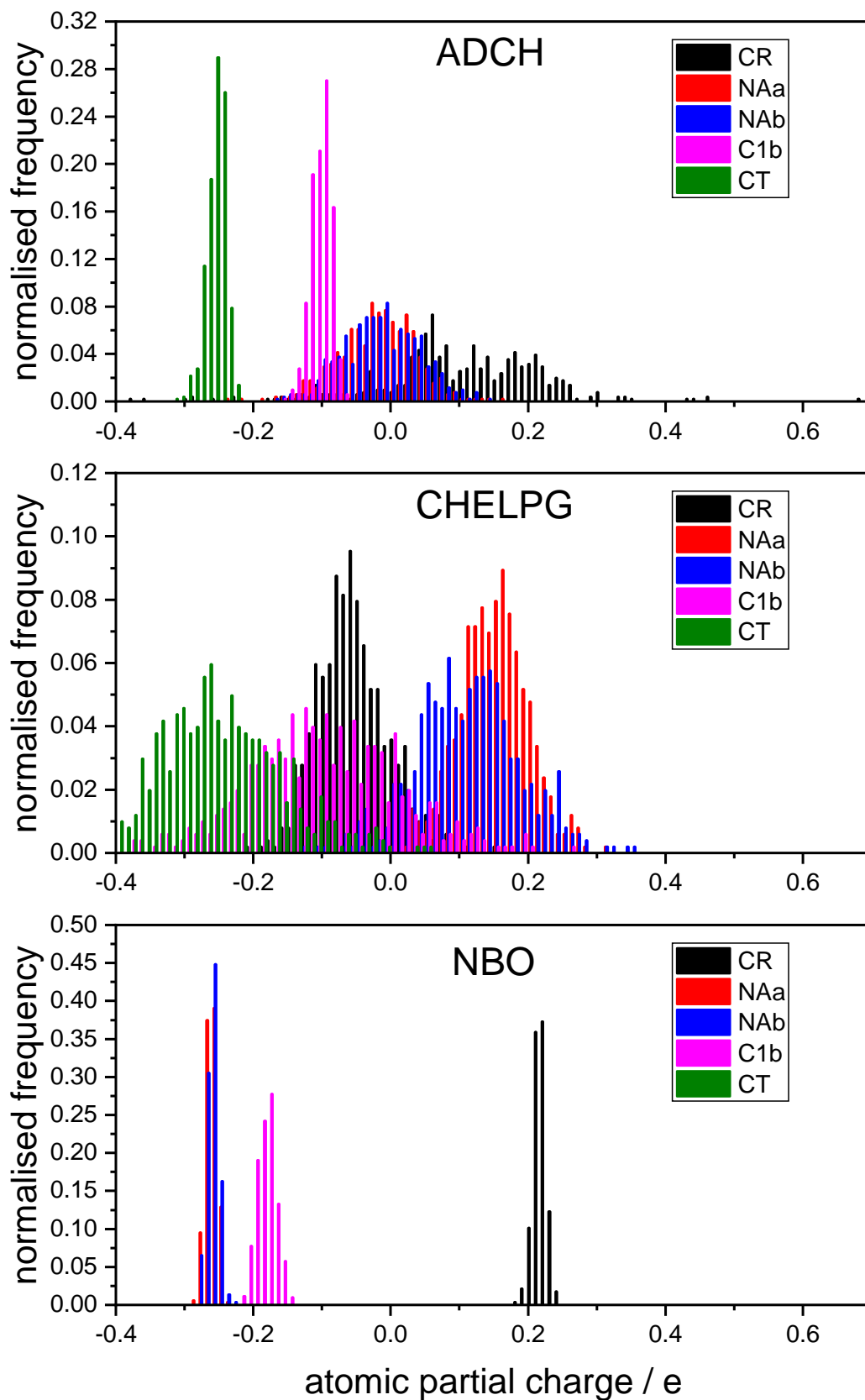
Figure S12: Histogram of atomic charges obtained for the $[C_4C_1Im]^+$ cation using different atomic charge partition schemes for th 512 structures sampled from the MD simulation.

13. ESP reproducibility

We use the Multiwfn[13] software to visualise the reproducibility of the electrostatic potential (ESP) generated by the averaged sets of atomic charges at the example of the trans conformer of the [NTf$_2$]$^-$ anion. The orientation is always the same as shown in Figure S13a without and in Figure S13b with grid points. The error in the ESP is given as root mean square error in Table S18, together with a visualisation of the error. Note that the ESP fitted charges are optimised for the grids employed, while this is not the case for the ADCH charges.
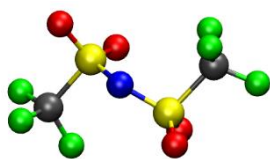
a)   b)
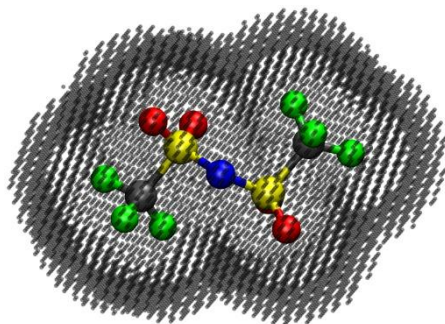
Figure S13: orientation of the [NTf2]– anion for the ESP reproducibility plots.

Table S18: ESP reproducibility plots using MSK (left column) and CHELPG (right column) grid points. The colour scale is green-white-red, from green = 0 kJ/mol error in the ESP to red = 12.6 kJ/mol (3 kcal/mol) error in the ESP, see the colour scale below. White corresponds to 6.3 kJ/mol (1.5 kcal/mol) error in the ESP.

MSK grid	CHELPG grid
CHELPG charges, RMSE=0.003095	CHELPG charges, RMSE=0.003534
MSK charges, RMSE=0.003433	MSK charges, RMSE=0.003984
ADCH charges, RMSE=0.004265	ADCH charges, RMSE=0.004841
NBO charges, RMSE=0.007935	NBO charges, RMSE=0.008065

0 kcal/mol   3 kcal/mol
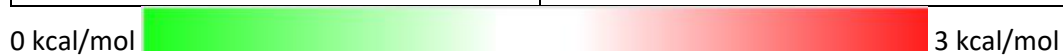
14.   Atomic charge interpolation for CHELPG

Figure S14 and Figure S15 show the interpolation of CHELPG atomic charges for cation and anion, respectively.
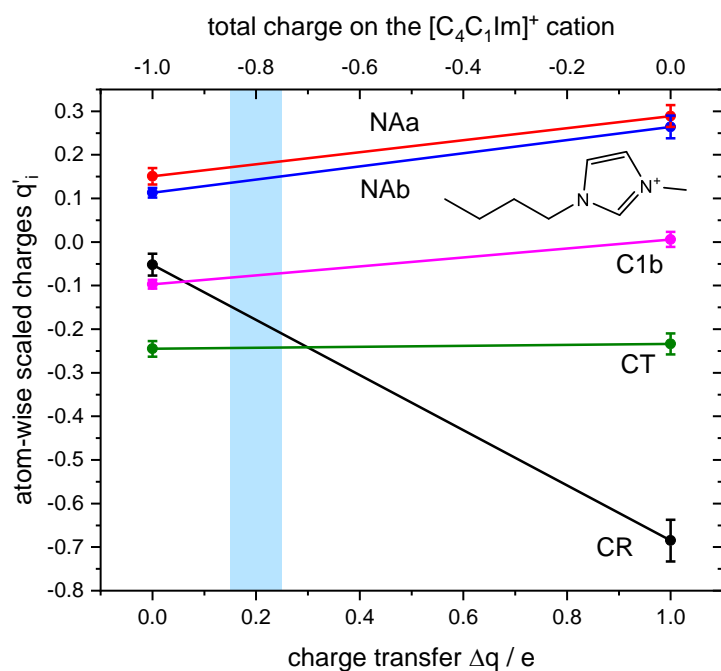
Figure S14: Interpolation of CHELPG atomic partial charges between the positively charged cation and the neutral radical. The shaded blue region corresponds to $\Delta q_{total} \approx 0.2$.
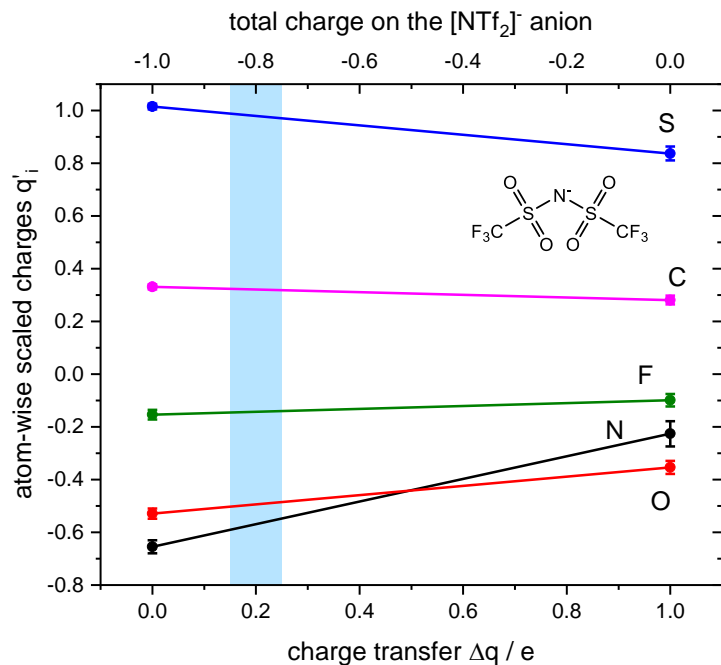
Figure S15: Interpolation of CHELPG atomic partial charges between the negatively charged anion and the neutral radical. The shaded blue region corresponds to $\Delta q_{total} \approx 0.2$.

15. Visualisation of charges, Fukui functions, orbitals

Figure S16 illustrates ESP based (CHELPG) charges and Fukui functions for vertical ionisation of the [NTf$_2$]$^-$ anion at the UMP2/cc-pVTZ//RB3LYP-GD3BJ/6-311+g(d,p) level of theory. The HOMO of the anion (Figure S17) and the LUMO of the cation (Figure S18) indicate regions of the molecular ions most susceptible to charge transfer.
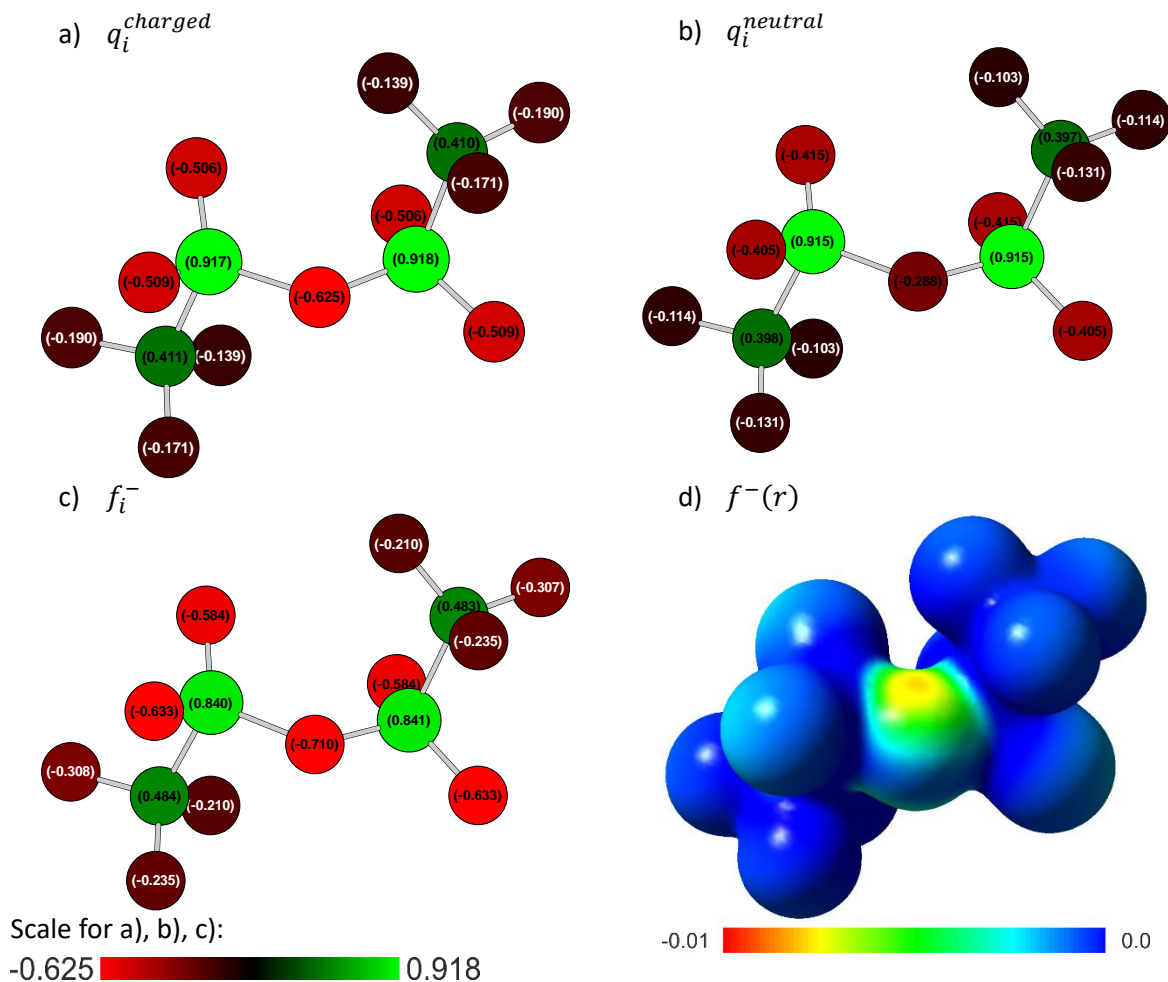
Figure S16: CHELPG atomic charges for a) the negatively charged anion, b) the corresponding neutral radical, c) the condensed finite difference Fukui function, d) Magnitude of the three-dimensional Fukui function mapped on the 0.02 isosurface of the anion electron density.

a) HOMO (canonical orbital)   b) HOMO (natural bond orbital)
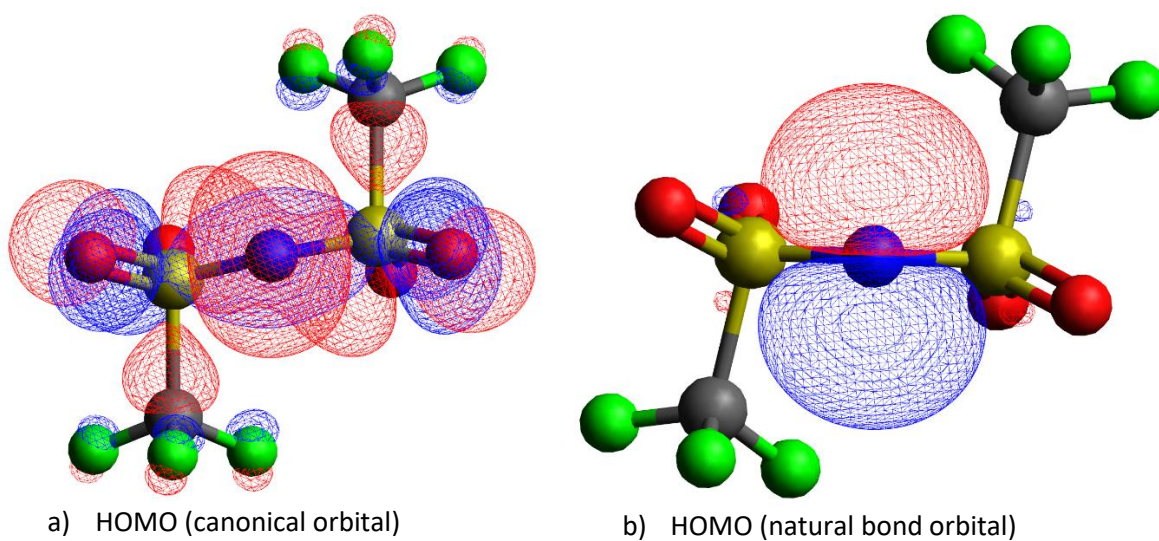
Figure S17: Highest occupied molecular orbital HOMO of the [NTf$_2$]$^-$ anion.

a) LUMO (canonical orbital)

b) LUMO (natural bond orbital)
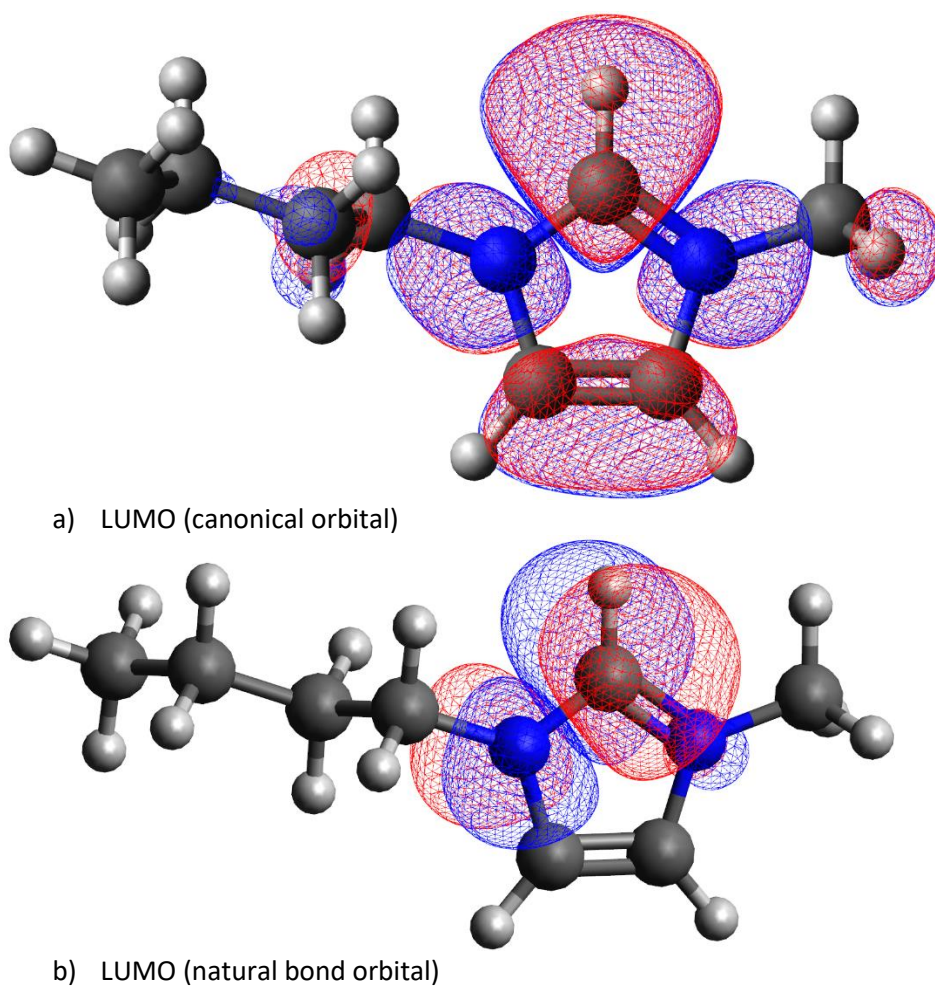
Figure S18: Lowest unoccupied molecular orbital LUMO of the [C$_4$C$_1$Im]$^+$ cation.

16. The Coulomb interaction energy

The Coulomb interaction energy between the ions (considered as point charges) is required to calculate the Coulomb correction and therefore the Madelung constant α. The screening conditions (sum rules) as described by McDaniel *et al.* are a convenient starting point for this calculation, Eqn (S20) for the cations C and Eqn (S21) for the anions A in a binary IL.[14,15] $g(r)$ are the pairwise radial distribution functions, ρ are the ideal densities, z is the charge of the considered ions. X are the cations C and anions A.

$$\int_0^\infty 4\pi r^2 \left[\sum_X z_X \rho_X g_X^C(r) \right] dr = -1 \tag{S20}$$

$$\int_0^\infty 4\pi r^2 \left[\sum_X z_X \rho_X g_X^A(r) \right] dr = +1 \tag{S21}$$

These two equations are the net neutrality conditions for a binary IL and must be strictly fulfilled. The sum rules can be interpreted in terms of n which is the (number) integral of a charge weighed radial distribution function g_{all} which considers all charged particles other than the central reference ion, Eqn (S22) and (S23). Here, $\rho_{all} = \rho_C + \rho_A$ is the overall particle density.

$$n^C(r') = \int_0^{r'} 4\pi r^2 \frac{\rho_{all}}{2} g_{all}^C(r) dr \tag{S22}$$

$$n^A(r') = \int_0^{r'} 4\pi r^2 \frac{\rho_{all}}{2} g_{all}^A(r) dr \tag{S23}$$

The total coulomb interaction energy with a central reference ion is due to all other ions (within an infinitesimal shell of radius r around the reference ion) and is given by $dU = ze \cdot V_E(r)n(r)dr$, with $V_E = {}^q/_{4\pi\varepsilon_0 r}$ being the Coulomb potential and z the charge of the reference ion. The approach leads to Eqn (S24) and Eqn (S25) and is equivalent to the derivation of the energy equation and excess energies from pair distribution functions.[16] The total Coulomb interaction energy is then the sum of the two components, Eqn (S26).

$$U^C = \int_0^\infty \frac{+e^2}{2\varepsilon_0} r \rho_{all} g_{all}^C(r) dr \tag{S24}$$

$$U^A = \int_0^\infty \frac{-e^2}{2\varepsilon_0} r \rho_{all} g_{all}^A(r) dr \tag{S25}$$

$$U^C + U^A = \frac{-\alpha e^2}{4\pi\varepsilon_0 d} \tag{S26}$$

17. Radial distribution functions

Radial distribution functions were calculated with TRAVIS using the centre of mass positions of ions.[17,18] The distance r, value of the radial distribution function g(r) and corresponding number integral for the relevant extrema are given in Table S19 (cation-cation RDF), Table S20 (cation-anion RDF) and Table S21 (anion-anion RDF).

Table S19: First two maxima and minima of the cation-cation radial distribution functions.

	First maximum			First minimum			Second maximum			Second minimum		
	r / Å	g(r)	n(r)	r / Å	g(r)	n(r)	r / Å	g(r)	n(r)	r / Å	g(r)	n(r)
CLP_ADCH_scaled	8.59	1.19	3.96	13.92	0.89	21.59	17.12	1.07	40.96	21.07	0.97	77.38
CLP_ADCH_unscaled	8.37	1.29	3.63	13.49	0.87	19.92	16.59	1.09	37.73	20.43	0.96	71.68
CLP_CHELPG_scaled	8.48	1.24	3.76	13.60	0.88	20.19	17.01	1.07	40.29	20.85	0.96	75.26
CLP_CHELPG_unscaled	8.48	1.32	3.92	13.17	0.87	18.58	16.37	1.09	36.35	20.21	0.95	69.62
CLP_MSK_scaled	8.48	1.21	3.74	13.71	0.88	20.72	17.01	1.07	40.29	21.07	0.96	77.67
CLP_MSK_unscaled	8.27	1.31	3.41	13.39	0.87	19.43	16.37	1.09	36.35	20.11	0.95	68.56
CLP_original	8.27	1.34	3.42	13.07	0.86	18.17	16.37	1.10	36.41	20.11	0.95	68.64
CLP_original_scaled	8.27	1.30	3.31	13.49	0.87	19.63	16.69	1.08	38.00	20.64	0.96	72.99
CL&P+Drude/TG-NH (C-H fix)	8.32	1.18	3.56	13.80	0.91	21.54	17.10	1.05	41.84	20.92	0.97	77.58
CL&Pol/TG-NH (C-H fix)	10.04	1.19	7.53	13.96	0.89	21.75	17.29	1.05	41.91	21.29	0.98	79.46

Table S20: First two maxima and minima of the cation-anion radial distribution functions.

	First maximum			First minimum			Second maximum			Second minimum		
	r / Å	g(r)	n(r)	r / Å	g(r)	n(r)	r / Å	g(r)	n(r)	r / Å	g(r)	n(r)
CLP_ADCH_scaled	5.49	2.29	1.15	9.55	0.63	7.39	12.53	1.19	16.13	16.91	0.93	40.68
CLP_ADCH_unscaled	5.39	2.44	1.16	9.55	0.61	7.32	12.43	1.25	16.08	16.37	0.91	37.64
CLP_CHELPG_scaled	5.49	2.23	1.26	9.55	0.63	7.30	12.64	1.20	16.73	16.91	0.91	40.69
CLP_CHELPG_unscaled	5.28	2.36	1.10	9.44	0.62	7.06	12.32	1.25	15.72	16.37	0.89	37.63
CLP_MSK_scaled	5.49	2.22	1.20	9.55	0.62	7.37	12.64	1.20	16.72	16.91	0.92	40.79
CLP_MSK_unscaled	5.39	2.37	1.22	9.55	0.61	7.28	12.43	1.26	16.18	16.37	0.90	37.68
CLP_original	5.39	2.36	1.26	9.44	0.61	7.07	12.21	1.26	15.26	16.16	0.90	36.35
CLP_original_scaled	5.39	2.26	1.12	9.55	0.62	7.25	12.53	1.22	16.33	16.69	0.91	39.23
CL&P+Drude/TG-NH (C-H fix)	5.53	2.14	1.26	9.45	0.64	7.33	12.35	1.17	15.79	16.79	0.94	40.73
CL&Pol/TG-NH (C-H fix)	5.54	2.16	1.15	9.46	0.65	7.23	12.71	1.14	16.81	17.38	0.95	43.77

Table S21: First two maxima and minima of the anion-anion radial distribution functions.

	First maximum			First minimum			Second maximum			Second minimum		
	r / Å	g(r)	n(r)	r / Å	g(r)	n(r)	r / Å	g(r)	n(r)	r / Å	g(r)	n(r)
CLP_ADCH_scaled	8.37	1.55	3.56	13.17	0.81	18.14	16.48	1.13	36.41	20.21	0.95	68.34
CLP_ADCH_unscaled	8.27	1.73	3.44	12.96	0.78	17.41	16.05	1.17	34.09	19.68	0.92	64.13
CLP_CHELPG_scaled	8.37	1.60	3.58	12.96	0.77	17.30	16.27	1.15	34.98	20.00	0.93	66.41
CLP_CHELPG_unscaled	8.27	1.77	3.44	12.75	0.74	16.59	16.05	1.21	34.28	19.57	0.90	63.27
CLP_MSK_scaled	8.37	1.59	3.60	13.07	0.79	17.73	16.27	1.15	34.99	20.11	0.94	67.53
CLP_MSK_unscaled	8.37	1.76	3.77	12.96	0.76	17.39	16.05	1.19	34.20	19.57	0.91	63.36
CLP_original	8.27	1.73	3.53	12.96	0.76	17.37	15.95	1.19	33.50	19.47	0.91	62.41
CLP_original_scaled	8.27	1.63	3.36	12.96	0.78	17.27	16.16	1.16	34.28	20.00	0.93	66.40
CL&P+Drude/TG-NH (C-H fix)	8.22	1.51	3.43	12.97	0.83	17.72	16.17	1.11	35.11	19.89	0.95	66.63
CL&Pol/TG-NH (C-H fix)	8.21	1.40	3.27	13.38	0.85	18.90	16.46	1.09	35.92	20.21	0.97	67.94

18. Coulomb interaction energy plot

The Coulomb interaction energy as a function of distance, according to Eqn (S24) to (S26), is shown in Figure S19.
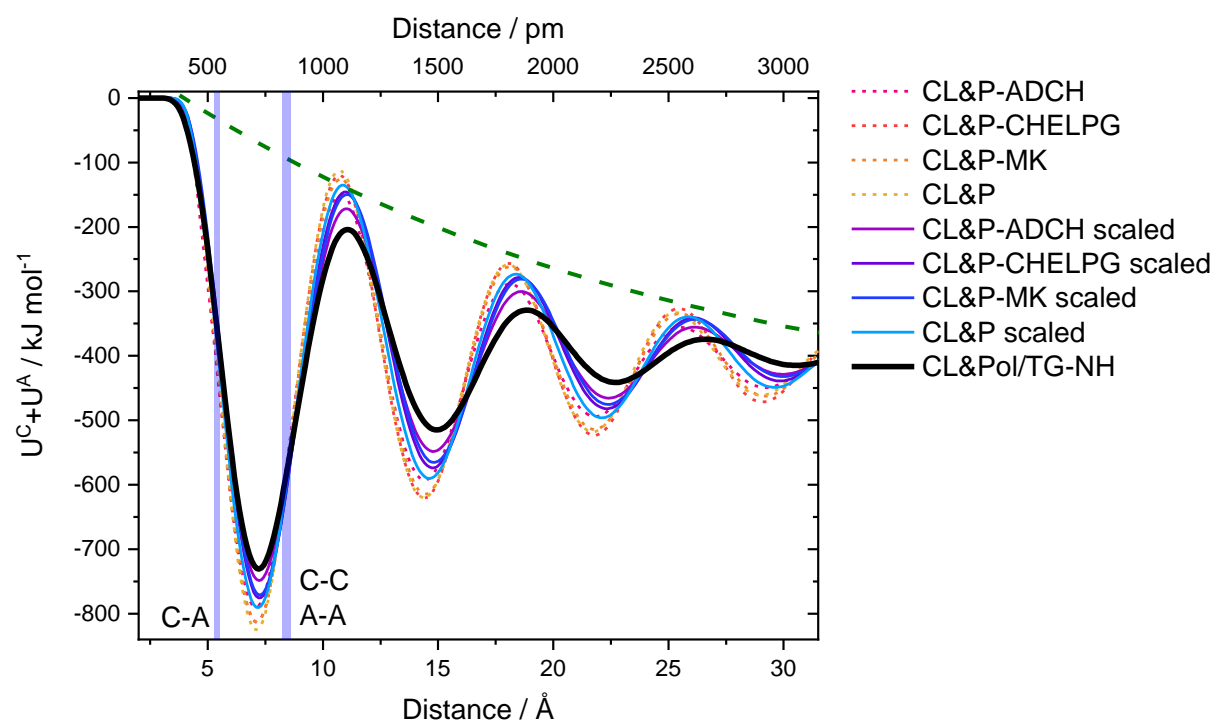
Figure S19: Coulomb interaction energy for cation+anion in [C4C1im][NTf2] as a function of distance, calculated using ±1 point charges at the centre of charge. The green dashed line shows an exponential envelope. The blue shaded areas correspond to the positions of the first maxima in the cation-anion RDFs (around 5.5 Å) and the cation-cation (C-C) and anion-anion (A-A) RDFs (around 8.5 Å).

19. Fit of coulomb interaction energy

The Coulomb interaction energy as a function of distance r was fitted with Eqn (S27). Small differences are obtained when the reference charge is identified at the centre of charge or the centre of mass, see fit parameters in The asymptotic long-distance limit value of $U = E_0$ is the energy required to fully separate the ions within the liquid, which ranges from −396 to −411 kJ/mol for the simulations undertaken here. Evaluating U at a distance of 5.28-5.54 Å (maximum of the cation-anion radial distribution functions, C-A shaded blue region in Figure S19) gives a Coulomb interaction energy between -360 kJ/mol and -400 kJ/mol, Table S24. (This result is semi-quantitative since U is evaluated relative to the centre of charge, and the RDF is here evaluated via the centre of mass) For reference, the interaction energy for a single ion pair in the gas phase (ie $\alpha=1$) is 250 kJ/mol (± 1 point charges, 5.5 Å apart, which is a typical value for the first peak in the cation-anion RDF). Thus the energy required to evaporate associated ions in the liquid phase into gas-phase ion pairs is approximately 110 to 150 kJ mol^{-1}. This value in in good agreement with the experimental heat of evaporation of [C$_4$C$_1$im][NTf$_2$] (130-140 kJ mol^{-1}) reported in the literature.[19,20]

Table S22 (for centre of charge) and Table S23 (for centre of mass). The charge transfer estimates obtained using E_0 are also given, the error in Δq is 0.02 e based on the errors in μ and η.

$$U^C(r) + U^A(r) = E_0 + A \exp\left(-\frac{r}{\lambda_D}\right) \sin\left(\frac{\pi(r - \varphi)}{w}\right) \qquad \text{(S27)}$$

The asymptotic long-distance limit value of $U = E_0$ is the energy required to fully separate the ions within the liquid, which ranges from −396 to −411 kJ/mol for the simulations undertaken here. Evaluating U at a distance of 5.28-5.54 Å (maximum of the cation-anion radial distribution functions, C-A shaded blue region in Figure S19) gives a Coulomb interaction energy between -360 kJ/mol and -400 kJ/mol, Table S24. (This result is semi-quantitative since U is evaluated relative to the centre of charge, and the RDF is here evaluated via the centre of mass) For reference, the interaction energy for a single ion pair in the gas phase (ie α=1) is 250 kJ/mol ($\pm$1 point charges, 5.5 Å apart, which is a typical value for the first peak in the cation-anion RDF). Thus the energy required to evaporate associated ions in the liquid phase into gas-phase ion pairs is approximately 110 to 150 kJ mol[-1]. This value in in good agreement with the experimental heat of evaporation of [C$_4$C$_1$im][NTf$_2$] (130-140 kJ mol^{-1}) reported in the literature.[19,20]

Table S22: Coulomb interaction energy fit parameters, using the centre of charge as the position of the ±1 point charges of the ions.

	E_0 / kJ mol^{-1}		φ / Å		w / Å	
	Value	Error	Value	Error	Value	Error
ADCH scaled	-399.365	0.204	1.691	0.003	3.791	0.002
ADCH unscaled	-410.781	0.266	1.661	0.004	3.689	0.002
CHELPG scaled	-398.605	0.259	1.731	0.004	3.764	0.002
CHELPG unscaled	-410.333	0.276	1.698	0.004	3.665	0.001
MSK scaled	-396.020	0.273	1.747	0.004	3.776	0.002
MSK unscaled	-408.529	0.299	1.716	0.004	3.671	0.002
CL&P unscaled	-408.535	0.309	1.734	0.004	3.649	0.002
CL&P scaled	-403.450	0.259	1.703	0.004	3.730	0.001
CL&Pol/TG-NH (C-H fix)	-398.409	0.252	1.635	0.005	3.858	0.002

Table S22 continued.

	λ_D / Å		A / kJ mol^{-1}		Adj. R^2	Δq / e
	Value	Error	Value	Error		Value
ADCH scaled	9.25	0.03	751093	3127	0.9993	-0.07
ADCH unscaled	10.00	0.04	760471	3647	0.9991	-0.09
CHELPG scaled	10.20	0.04	750631	3484	0.9991	-0.07
CHELPG unscaled	11.79	0.05	722357	3105	0.9992	-0.09
MSK scaled	9.87	0.04	764759	3839	0.9990	-0.07
MSK unscaled	11.18	0.05	748641	3579	0.9990	-0.09
CL&P unscaled	11.03	0.05	779826	3756	0.9990	-0.09

| CL&P scaled | 10.58 | 0.04 | 750702 | 3325 | 0.9992 | -0.08 |
| CL&Pol/TG-NH (C-H fix) | 7.59 | 0.04 | 848656 | 5278 | 0.9987 | -0.07 |

Table S23: Coulomb interaction energy fit parameters, using the centre of mass as the position of the ±1 point charges of the ions.

	E_0 / kJ mol^{-1}		φ / Å		w / Å	
	Value	Error	Value	Error	Value	Error
ADCH scaled	-363.598	0.249	2.000	0.004	3.806	0.002
ADCH unscaled	-375.569	0.292	1.939	0.004	3.707	0.002
CHELPG scaled	-371.625	0.223	1.924	0.004	3.785	0.002
CHELPG unscaled	-383.964	0.267	1.885	0.004	3.675	0.001
MSK scaled	-368.037	0.226	1.963	0.004	3.794	0.002
MSK unscaled	-380.106	0.254	1.923	0.004	3.684	0.001
CL&P unscaled	-381.558	0.291	1.896	0.004	3.669	0.002
CL&P scaled	-373.985	0.270	1.913	0.004	3.746	0.002
CL&Pol/TG-NH (C-H fix)	-361.630	0.181	1.978	0.003	3.772	0.002

Table S23 continued.

	λ_D / Å		A / kJ mol^{-1}		Adj. R^2	Δq / e
	Value	Error	Value	Error		Value
ADCH scaled	8.90	0.04	759802	4118	0.9989	-0.01
ADCH unscaled	9.63	0.05	775527	4292	0.9988	-0.03
CHELPG scaled	9.90	0.04	721158	3184	0.9992	-0.03
CHELPG unscaled	11.42	0.05	692551	3169	0.9991	-0.05
MSK scaled	9.61	0.04	729310	3346	0.9992	-0.02
MSK unscaled	10.85	0.04	720496	3204	0.9992	-0.04
CL&P unscaled	10.69	0.05	730859	3737	0.9989	-0.04
CL&P scaled	10.32	0.05	709841	3649	0.9989	-0.03
CL&Pol/TG-NH (C-H fix)	7.69	0.03	814088	3705	0.9993	-0.01

Table S24: Asymptotic limit for both the centre of mass and centre of charge as the position of the ±1 point charges of the ions and the corresponding α and charge transfer values.

	RDF	CoM			CoC		
	r_{max}(C-A) /Å	E_0 / kJ mol^{-1}	α	Δq / e	E_0 / kJ mol^{-1}	α	Δq / e
ADCH scaled	5.49	-363.598	1.44	-0.01	-399.365	1.58	-0.07
ADCH unscaled	5.39	-375.569	1.46	-0.03	-410.781	1.59	-0.09
CHELPG scaled	5.49	-371.625	1.47	-0.03	-398.605	1.58	-0.07
CHELPG unscaled	5.28	-383.964	1.46	-0.05	-410.333	1.56	-0.09
MSK scaled	5.49	-368.037	1.45	-0.02	-396.020	1.56	-0.07
MSK unscaled	5.39	-380.106	1.47	-0.04	-408.529	1.58	-0.09
CL&P unscaled	5.39	-381.558	1.48	-0.04	-408.535	1.58	-0.09
CL&P scaled	5.39	-373.985	1.45	-0.03	-403.450	1.57	-0.08
CL&Pol/TG-NH (C-H fix)	5.53	-361.630	1.44	-0.01	-398.409	1.59	-0.07

20. Nernst-Einstein

The Nernst-Einstein equation is used to describe ionic conduction within low concentration salts. It is well recognised that the equation does not recover the full physics for concentrated electrolyte. However, this equation is a good starting point for more sophisticated models. The Nernst-Einstein equation relates the molar conductivity (Λ_{self}) to the charge on each ion (z^i=1 for ILs) ,Faraday constant (F), temperature (T), gas constant (R) and the sum of the self diffusion coefficients of the individual ions D^i, Eqn (S28).

$$\Lambda_{self} = \frac{F^2}{RT} \sum_i \left(z^i\right)^2 D_{self}^i = \frac{F^2}{RT} \left(D_{self}^C + D_{self}^A \right) \tag{S28}$$

In concentrated salt solutions or ionic liquids, the assumption of a limiting infinitely dilute solution breaks down and in many cases the experimentally determined molar conductivity differs from that predicted. A correction factor reducing the molar conductivity, via the Nernst-Einstein deviation parameter Δ_{NE}, where the quantity $(1 - \Delta_{NE})$ is interpreted as "ionicity" (or Haven ratio) can be introduced, Eqn (S29).

$$\Lambda_{exp.} = (1 - \Delta_{NE})\Lambda_{self} \tag{S29}$$

Different rationalisations for deviations from the Nernst-Einstein equation have been explored. One interpretation is based on the assumption that the lower experimental conductivity is due to transient or static ion pairing or ion aggregation, forming neutral or reduced charge clusters (reducing the number of charge carriers).[21–23] Alternatively, ion-ion (anti)correlated motions in the presence of an electric field can be introduced through cross correlation terms, breaking down the assumption that diffusion can be simply represented as a sum of self-diffusion coefficients.[24,25] This leads to an additional term in the molar conductivity where D_d are distinct diffusion coefficients, Eqn (S30).

$$\Lambda_{\text{cross}} = \frac{F^2}{RT}\left(\frac{1}{2}D_d^{CC} + \frac{1}{2}D_d^{AA} - D_d^{CA}\right) \tag{S30}$$

Another approach rationalises deviations from the Nernst-Einstein equation as due to charge transfer which reduces the charges z^i, leading to an experimentally accessible estimate of charge transfer of $\Delta q = 1 - \sqrt{1 - \Delta_{\text{NE}}}$, where Δq is the average charge transfer from anion to cation.[26] Combining the concepts of cross correlation contributions with the potential for non-integer charges leads to Eqn (S31).

$$\Lambda_{\text{theoretical}} = (1 - \Delta q)^2(\Lambda_{\text{self}} + \Lambda_{\text{cross}}) \tag{S31}$$

Equating the theoretical and experimental molar conductivity, Eqn (S32).

$$(1 - \Delta_{\text{NE}})\Lambda_{\text{self}} = (1 - \Delta q)^2(\Lambda_{\text{self}} + \Lambda_{\text{cross}}) \tag{S32}$$

This leads to Eqn (S33) to (S35).

$$(1 - \Delta_{\text{NE}}) = (1 - 2\Delta q + \Delta q^2)\left(1 + \frac{\Lambda_{\text{cross}}}{\Lambda_{\text{self}}}\right) \tag{S33}$$

$$\Delta q^2 - 2\Delta q + 1 - \frac{1 - \Delta_{\text{NE}}}{1 + \frac{\Lambda_{\text{cross}}}{\Lambda_{\text{self}}}} = 0 \tag{S34}$$

$$\Delta q = 1 \pm \sqrt{\frac{1 - \Delta_{\text{NE}}}{1 + \frac{\Lambda_{\text{cross}}}{\Lambda_{\text{self}}}}} \tag{S35}$$

The strength of this equation is that it requires only ratios to be calculated from either experiment or theory. The 'real' conductivity used in Δ_{NE} is only experimentally accessible, and the cross contribution Λ_{cross} is only theoretically accessible. Only the solution which yields charge transfer <1 will be considered. Importantly, if the cross contributions Λ_{cross} are zero, then this equation recovers $\Delta q = 1 - \sqrt{1 - \Delta_{\text{NE}}}$.

However, computation of the distinct diffusion coefficients needed to evaluate Λ_{cross} comes at considerable computational cost. Instead, we will use the diffusion coefficient obtained from the integral of the relative mean molecular velocity correlation function $D_{RMMVCF}^{C,A}$, Eqn (S36).[27–30]

$$D_{RMMVCF}^{C,A} = \frac{N}{12}\int_0^\infty \langle(\vec{\boldsymbol{u}}^C(t) - \vec{\boldsymbol{u}}^A(t)) \cdot (\vec{\boldsymbol{u}}^C(0) - \vec{\boldsymbol{u}}^A(0))\rangle dt \tag{S36}$$

Here, N is the total number of ions, i.e. the sum of the number of cations N^C and the number of anions N^A. $\vec{\boldsymbol{u}}^C$ and $\vec{\boldsymbol{u}}^A$ are the mean molecular velocities of all the cations and anions, respectively, Eqn (S37) & (S38) where $\vec{u}_i$ is the velocity of the centre of mass of one particular ion.

$$\vec{\boldsymbol{u}}^C(t) = \frac{1}{N^C} \sum_{i=1}^{N^C} \vec{u}_i^C(t) \tag{S37}$$

$$\vec{\boldsymbol{u}}^A(t) = \frac{1}{N^A} \sum_{i=1}^{N^A} \vec{u}_i^A(t) \tag{S38}$$

$D_{RMMVCF}^{C,A}$ is related to the distinct cross contributions as shown in (S39).[28,30]

$$D_{RMMVCF}^{C,A} = \frac{1}{2}\left(D_{self}^C + D_{self}^A\right) + \frac{1}{2}\left(\frac{1}{2}D_d^{CC} + \frac{1}{2}D_d^{AA} - D_d^{CA}\right) \tag{S39}$$

Which, in combination with (S30), leads to (S40).

$$\frac{\Lambda_{\text{cross}}}{\Lambda_{\text{self}}} = \frac{2D_{RMMVCF}^{C,A}}{D_{self}^C + D_{self}^A} - 1 \tag{S40}$$

In this work, we first calculated the diffusion coefficients for $\frac{\Lambda_{\text{cross}}}{\Lambda_{\text{self}}}$ using the Green-Kubo expression. This has the disadvantage that both very short sampling intervals and long simulation runs are required. In our case, we used a total of 1000 ns simulation time, with velocities written every 20 fs, leading to a relatively high storage requirement (>35 TB). We thus recommend the use of the corresponding Einstein relation, Eqn (S41), which is mathematically equivalent to the Green-Kubo expression.[4] Here, N is the total number of ions, x^C and x^A are the mole fraction of cation and anions, respectively.

$$D_{\{RMM\}}^{\{C,A\}} = \frac{1}{6}Nx^Cx^A \lim_{t\to\infty} = \frac{d}{dt}\langle\left(\vec{r}^C(t) - \vec{r}^A(t)\right) - \left(\vec{r}^C(0) - \vec{r}^A(0)\right)\rangle^2 \tag{S41}$$

Here, $\vec{r}$ are the mean molecular positions, defined in Eqn (S42) and (S43)

$$\vec{r}^C(t) = \frac{1}{N^C} \sum_{i=1}^{N^C} \vec{r}_i^C(t) \tag{S42}$$

$$\vec{r}^A(t) = \frac{1}{N^A} \sum_{i=1}^{N^A} \vec{r}_i^A(t) \tag{S43}$$

Future work could include analysing mixtures with an increasing contribution from a molecular solvent, which are anticipated to smoothly turn off charge transfer and the influence of cross-contributions.

Green-Kubo diffusion coefficients were obtained by fitting the integrated correlation functions from 30 ps to 4 ns with a monoexponential function Eqn (S44), a biexponential function Eqn (S45), or a stretched exponential, Eqn (S46). The Einstein diffusion coefficients were obtained via the slope of linear fits of the corresponding mean squared displacements.

$$y = A_1 \exp\left(-\frac{x}{t_1}\right) + y_0 \tag{S44}$$

$$y = A_1 \exp\left(-\frac{x}{t_1}\right) + A_2 \exp\left(-\frac{x}{t_2}\right) + y_0 \tag{S45}$$

$$y = A_1 \exp\left(-\frac{x^\beta}{t_1}\right) + y_0 \tag{S46}$$

21. Visualisation of domain formation

No pronounced aggregation of apolar groups is visible in the Portuguese flag plot shown in Figure S20. The snapshot was generated with VMD in orthographic view, wrapped molecule-wise using TRAVIS.[17,31]
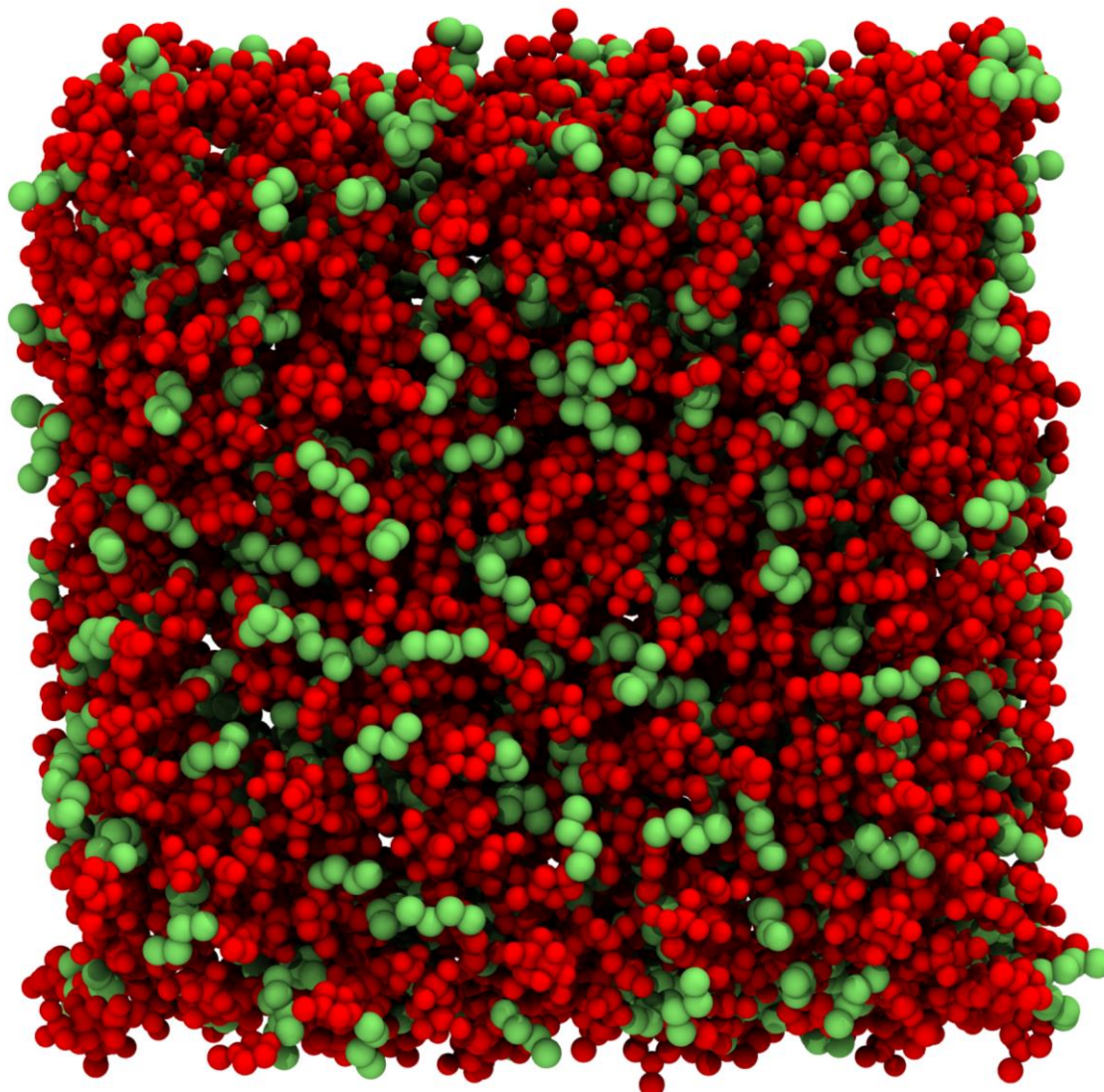
Figure S20: Snapshot of the first step in the trajectory of the CL&Pol/TG-NH simulation. Non-polar groups (the side chain of the $[C_4C_1im]^+$ cation) are coloured green, everything else is coloured red. Hydrogen atoms are omitted for clarity.

22.   Dihedral occurrences

The normalised frequency of dihedral angles in the [NTf$_2$]$^-$ anion as a function of the two backbone dihedral angles (2D histograms) is shown in Figure S21.
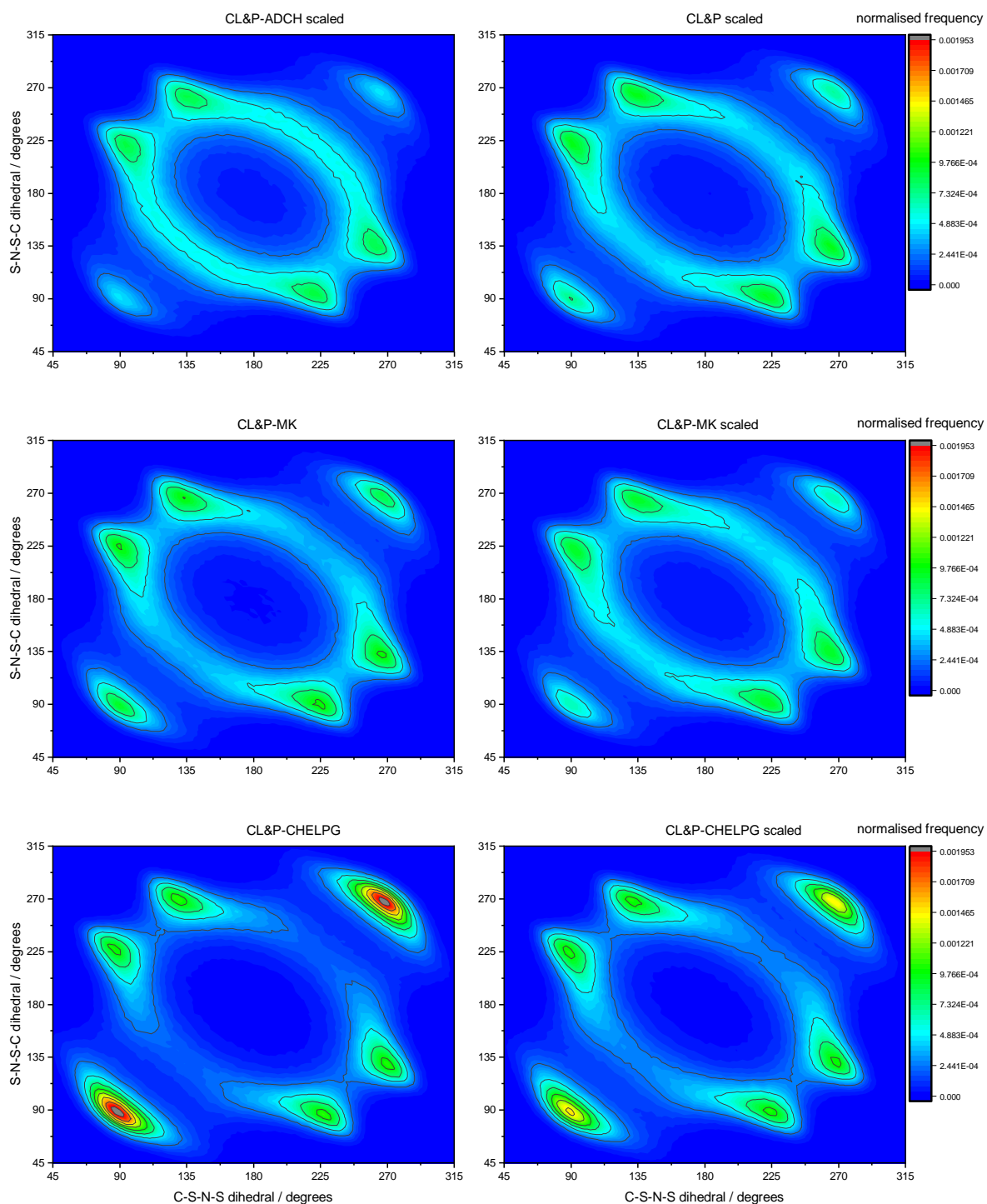
Figure S21: Occurrence of the two backbone dihedrals in the [NTf2]– anion.

23.   Dihedral potential energy surfaces

Figure S22 shows partially relaxed potential energy surfaces for the MP2/cc-pVTZ//RB3LYP-GD3BJ/6-311+G(d,p) level of theory, the CL&P force field, and the polarisable CL&Pol force field.
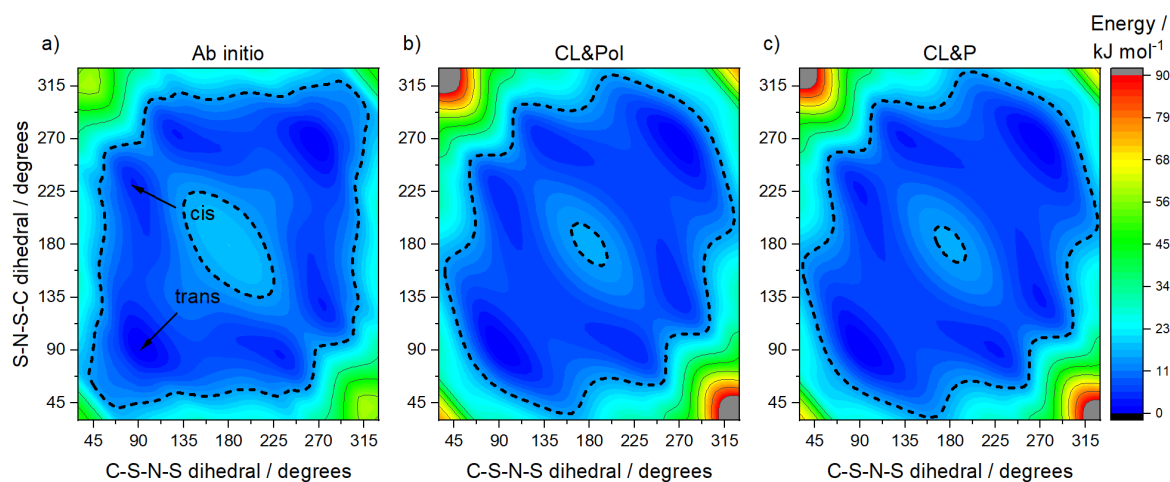
Figure S22: Potential energy surfaces for an isolated [NTf$_2$]$^-$ anion at different levels of theory. a) ab initio[32], b) CL&POL, c) CL&P.

24.   Charge arm distributions

Figure S23 shows the charge arm distribution for the force fields, including CHELPG unscaled, CHELPG scaled, and ADCH unscaled, which were omitted in the main paper to improve clarity. The ab initio charge arm lengths as a function of the two anion backbone dihedral angles are shown in Figure S24 and Figure S25.
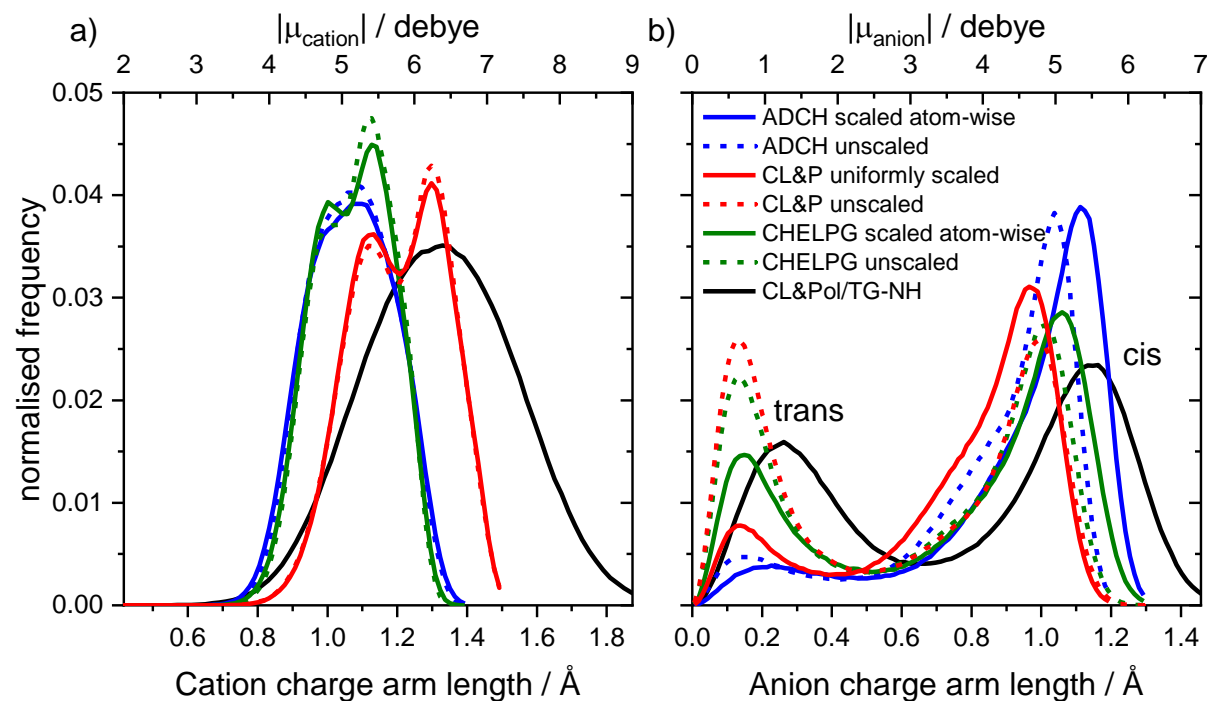
Figure S23: Charge arm distribution from the MD simulations.
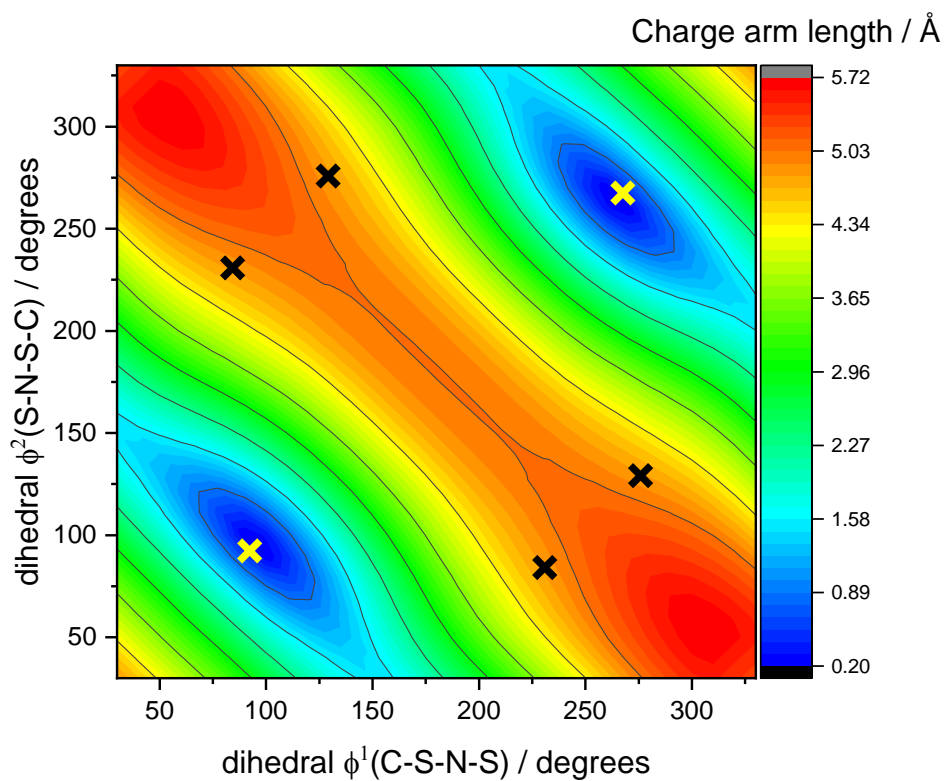
Figure S24: Charge arm lengths at the RB3LYP-GD3BJ/6-311+G(d,p) level of theory. Black crosses correspond to the cis geometry, yellow crosses correspond to the trans geometry.
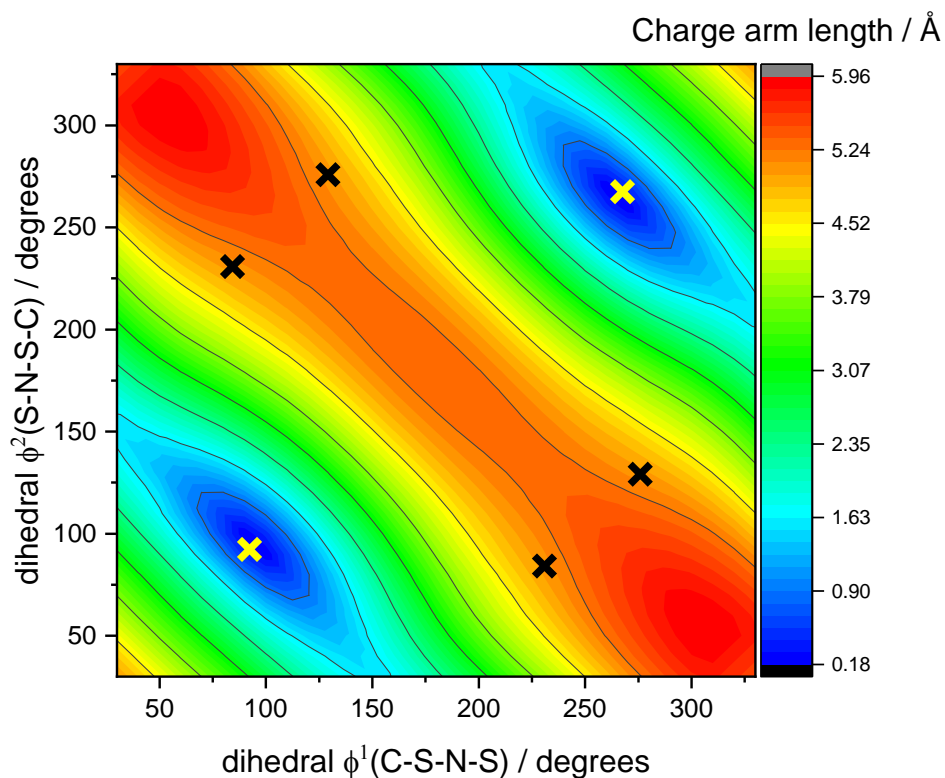
Figure S25: Charge arm lengths at the MP2/cc-pVTZ//RB3LYP-GD3BJ/6-311+G(d,p) level of theory. Black crosses correspond to the cis geometry, yellow crosses correspond to the trans geometry.

25. Diffusion coefficients, mean squared displacements

Diffusion coefficients were obtained by linear fits of the mean squared displacements from 3 to 7 ns as described in the main manuscript. A log-log-plot is suitable to identify cases of anomalous diffusion and at the same time serve as a check that the diffusive regime has been reached, Figure S26 and Figure S27. However, note that the ballistic regime is overemphasized in the MSD plots due to the logarithmic scale. The numerical values for diffusion coefficients from the fit can be found in Table S25 and Table S26.

That the diffusive regime is reached is evident visually in Figure S26 and Figure S27 by comparison with the green experimental line, which has a slope of 1 corresponding to normal diffusion. The exponent a can be obtained by fitting the mean squared displacement with Eqn (11) from the main manuscript, the resulting values are given in Table S27. However, these values have a relatively high uncertainty, see also the discussion of diffusion coefficients in the main manuscript. To illustrate this point, we fitted the x, y, and z components of the mean squared displacement of the scaled ADCH simulation with $\langle r^2(t) \rangle = 2Dt^a$, giving values of $a_x = 0.84$, $a_y = 1.01$ and $a_z = 0.84$. The standard deviation as a measure of uncertainty is 0.1, and $3\sigma = 0.3$. This confirms that the diffusive regime is reached, however within the relatively large error bars.
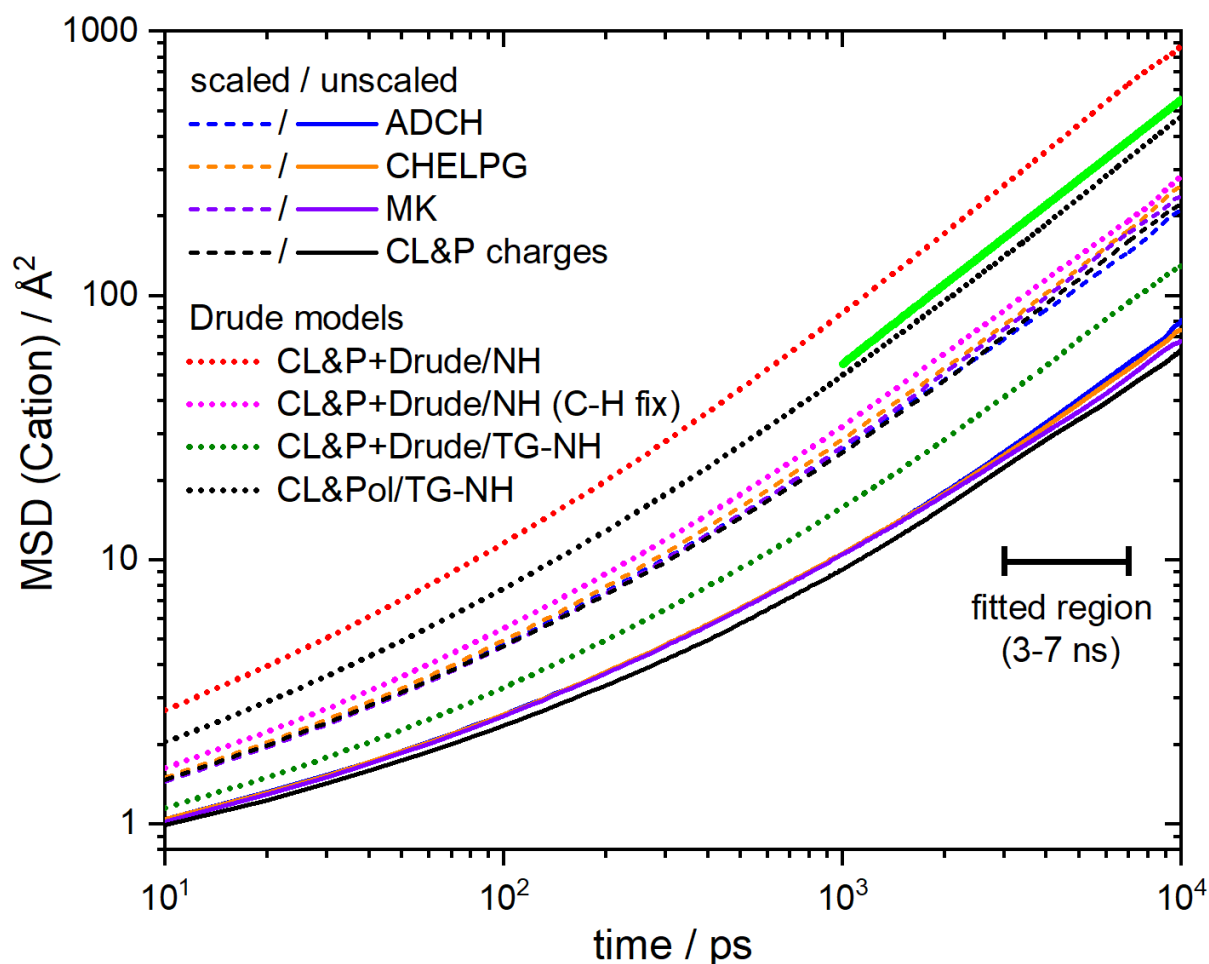
Figure S26: log-log plot of the mean squared displacements for the cation.
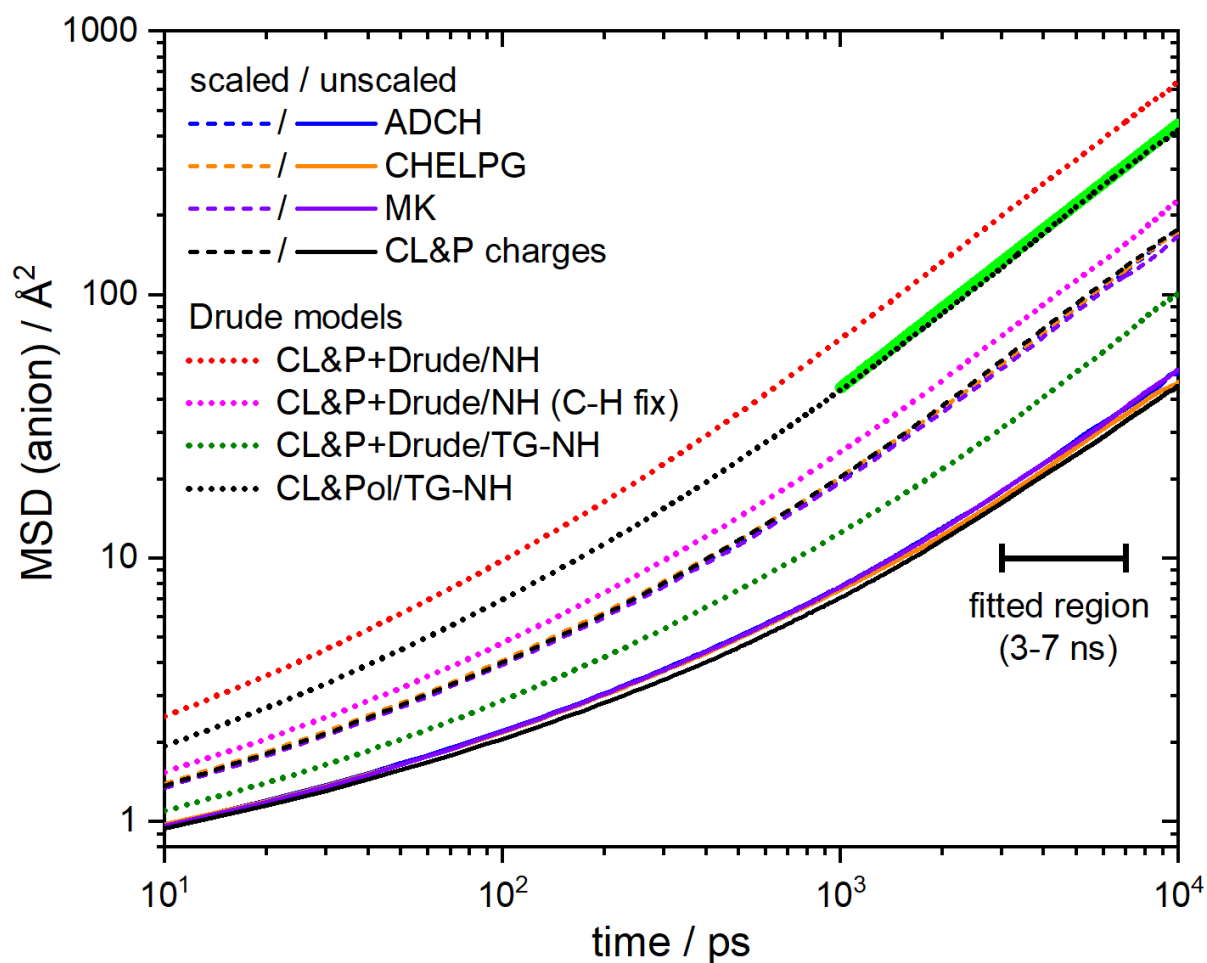
Figure S27: log-log plot of the mean squared displacements for the anion.

Table S25: Cation diffusion coefficients from the MD simulations.

	Intercept / Å^2		Slope / Å^2 fs^{-1}		Adj. R^2	Diffusion / m^2 s^{-1}	
	Value	Error	Value	Error		Value	Error
ADCH scaled	10.38	0.07	1.96E-05	1.42E-08	0.99979	3.26E-11	2.36E-14
ADCH unscaled	3.11	0.01	7.53E-06	1.21E-09	0.99999	1.25E-11	2.02E-15
CHELPG scaled	2.38	0.02	2.50E-05	4.43E-09	0.99999	4.17E-11	7.39E-15
CHELPG unscaled	4.02	0.02	7.03E-06	3.12E-09	0.99992	1.17E-11	5.20E-15
MSK scaled	-0.53	0.07	2.49E-05	1.36E-08	0.99988	4.16E-11	2.27E-14
MSK unscaled	5.94	0.02	6.15E-06	4.56E-09	0.99978	1.02E-11	7.60E-15
CL&P unscaled	6.20	0.03	5.57E-06	6.43E-09	0.99947	9.28E-12	1.07E-14
CL&P scaled	2.54	0.03	2.27E-05	6.38E-09	0.99997	3.78E-11	1.06E-14
CL&P+Drude/NH (no shake)	-21.11	0.20	9.36E-05	3.92E-08	0.99993	1.56E-10	6.53E-14
CL&P+Drude/NH (C-H fix)	10.38	0.11	2.63E-05	2.19E-08	0.99972	4.38E-11	3.66E-14
CL&P+Drude/TG-NH (C-H fix)	0.62	0.04	1.35E-05	8.10E-09	0.99986	2.25E-11	1.35E-14
CL&Pol/TG-NH (C-H fix)	-4.21	0.03	4.80E-05	6.00E-09	0.99994	8.00E-11	1.00E-14

Table S26: Anion diffusion coefficients from the MD simulations.

	Intercept / Å^2		Slope / Å^2 fs^{-1}		Adj. R^2	Diffusion / m^2 s^{-1}	
	Value	Error	Value	Error		Value	Error
ADCH scaled	2.89	0.04	1.72E-05	8.57E-09	0.99990	2.86E-11	1.43E-14
ADCH unscaled	3.66	0.04	4.85E-06	7.94E-09	0.99893	8.08E-12	1.32E-14
CHELPG scaled	0.35	0.08	1.79E-05	1.56E-08	0.99970	2.99E-11	2.60E-14
CHELPG unscaled	3.17	0.03	4.63E-06	5.32E-09	0.99947	7.72E-12	8.87E-15
MSK scaled	1.95	0.10	1.69E-05	1.87E-08	0.99951	2.81E-11	3.12E-14
MSK unscaled	3.66	0.02	4.80E-06	3.52E-09	0.99978	8.01E-12	5.87E-15
CL&P unscaled	3.83	0.01	4.20E-06	2.73E-09	0.99983	7.00E-12	4.54E-15
CL&P scaled	2.48	0.06	1.81E-05	1.08E-08	0.99986	3.01E-11	1.80E-14
CL&P+Drude/NH (no shake)	10.58	0.16	6.35E-05	3.17E-08	0.99990	1.06E-10	5.28E-14
CL&P+Drude/NH (C-H fix)	6.41	0.08	2.14E-05	1.64E-08	0.99976	3.57E-11	2.74E-14
CL&P+Drude/TG-NH (C-H fix)	0.86	0.03	1.00E-05	5.57E-09	0.99988	1.67E-11	9.28E-15
CL&Pol/TG-NH (C-H fix)	-5.90	0.03	4.44E-05	5.00E-09	0.00005	7.41E-11	8.33E-15

Table S27: Values for the exponent a, fitting the mean squared displacement with $\langle r^2(t)\rangle = 6Dt^a$ from 3-7 ns.

	Cation	Anion
ADCH scaled	0.90	0.97
ADCH unscaled	0.92	0.86
CHELPG scaled	0.98	0.99
CHELPG unscaled	0.89	0.87
MSK scaled	1.00	0.98
MSK unscaled	0.83	0.86
CL&P unscaled	0.81	0.84
CL&P scaled	0.98	0.97
CL&P+Drude/NH (no shake)	1.05	0.97
CL&P+Drude/NH (C-H fix)	0.92	0.94
CL&P+Drude/TG-NH (C-H fix)	0.99	0.98
CL&Pol/TG-NH (C-H fix)	1.02	1.03

26.   Performance of CL&Pol vs. CL&P

The performance of CL&P with fixed charges was 17.8 ns/day for 300 ion pair of [C$_4$C$_1$im][NTf$_2$] on an Intel 6226R Cascade Lake hexadeca-core 2.9 Ghz machine. For CL&Pol, the performance decreased to 3.2 ns/day. Both models had 99.7% CPU use with 32 MPI tasks.

27. References

[1]   K. R. Harris, M. Kanakubo, *Phys. Chem. Chem. Phys.* **2015**, *17*, 23977–23993.

[2]   E. J. Maginn, R. A. Messerly, D. J. Carlson, D. R. Roe, J. R. Elliott, *Living J. Comput. Mol. Sci.* **2019**, *1*, 1–20.

[3]   J. E. Basconi, M. R. Shirts, *J. Chem. Theory Comput.* **2013**, *9*, 2887–2899.

[4]   M. P. Allen, D. J. Tildesley, *Computer Simulation of Liquids*, Oxford University Press, **2017**.

[5]   B. Jeziorski, R. Moszynski, K. Szalewicz, *Chem. Rev.* **1994**, *94*, 1887–1930.

[6]   E. G. Hohenstein, C. D. Sherrill, *Wiley Interdiscip. Rev. Comput. Mol. Sci.* **2012**, *2*, 304–326.

[7]   K. Goloviznina, J. N. Canongia Lopes, M. Costa Gomes, A. A. H. Pádua, *J. Chem. Theory Comput.* **2019**, *15*, 5858–5871.

[8]   G. Lamoureux, B. Roux, *J. Chem. Phys.* **2003**, *119*, 3025–3039.

[9]   C. Y. Son, J. G. McDaniel, Q. Cui, A. Yethiraj, *J. Phys. Chem. Lett.* **2019**, *10*, 7523–7530.

[10]   A. Dequidt, J. Devémy, A. A. H. Pádua, *J. Chem. Inf. Model.* **2016**, *56*, 260–268.

[11]   V. S. Bernales, A. V. Marenich, R. Contreras, C. J. Cramer, D. G. Truhlar, *J. Phys. Chem. B* **2012**, *116*, 9122–9129.

[12]   P. Geerlings, F. De Proft, W. Langenaeker, *Chem. Rev.* **2003**, *103*, 1793–1874.

[13]   T. Lu, F. Chen, *J. Comput. Chem.* **2012**, *33*, 580–592.

[14]   J. G. McDaniel, A. Yethiraj, *J. Phys. Chem. B* **2019**, *123*, 3499–3512.

[15]   P. Keblinski, J. Eggebrecht, D. Wolf, S. R. Phillpot, *J. Chem. Phys.* **2000**, *113*, 282–291.

[16]   J.-P. Hansen, I. R. McDonald, in *Theory Simple Liq.*, Elsevier, **2013**, pp. 13–59.

[17]   M. Brehm, B. Kirchner, *J. Chem. Inf. Model.* **2011**, *51*, 2007–2023.

[18]   M. Brehm, M. Thomas, S. Gehrke, B. Kirchner, *J. Chem. Phys.* **2020**, *152*, 164105.

[19]   S. Horike, M. Ayano, M. Tsuno, T. Fukushima, Y. Koshiba, M. Misaki, K. Ishida, *Phys. Chem. Chem. Phys.* **2018**, *20*, 21262–21268.

[20]   B. Brunetti, A. Ciccioli, G. Gigli, A. Lapi, N. Misceo, L. Tanzi, S. Vecchio Ciprioti, *Phys. Chem. Chem. Phys.* **2014**, *16*, 15653.

[21]   G. W. Driver, Y. Huang, A. Laaksonen, T. Sparrman, Y.-L. Wang, P.-O. Westlund, *Phys. Chem. Chem. Phys.* **2017**, *19*, 4975–4988.

[22]   A. Rupp, N. Roznyatovskaya, H. Scherer, W. Beichel, P. Klose, C. Sturm, A. Hoffmann, J. Tübke, T. Koslowski, I. Krossing, *Chem. - A Eur. J.* **2014**, *20*, 9794–9804.

[23]   K. Ueno, H. Tokuda, M. Watanabe, *Phys. Chem. Chem. Phys.* **2010**, *12*, 1649–1658.

[24]   H. K. Kashyap, H. V. R. Annapureddy, F. O. Raineri, C. J. Margulis, *J. Phys. Chem. B* **2011**, *115*, 13212–13221.

[25]   K. R. Harris, *J. Phys. Chem. B* **2016**, *120*, 12135–12147.

[26]   F. Philippi, D. Rauber, M. Springborg, R. Hempelmann, *J. Phys. Chem. A* **2019**, *123*, 851–861.

[27]   J. Trullàs, J. A. Padró, *J. Chem. Phys.* **1993**, *99*, 3983–3989.

[28]   J. Trullàs, J. A. Padró, *Phys. Rev. E* **1994**, *50*, 1162–1170.

[29]   F. O. Raineri, H. L. Friedman, *J. Chem. Phys.* **1989**, *91*, 5633–5641.

[30]   J. Trullàs, J. A. Padró, *Phys. Rev. B* **1997**, *55*, 12210–12217.

[31]   W. Humphrey, A. Dalke, K. Schulten, *J. Mol. Graph.* **1996**, *14*, 33–38.

[32]   F. Philippi, D. Pugh, D. Rauber, T. Welton, P. A. Hunt, *Chem. Sci.* **2020**, *11*, 6405–6422.